THESIS FOR THE DEGREE OF LICENTIATE OF ENGINEERING

Towards electrified cement production

Modelling studies of heat transfer conditions in plasma-heated rotary kilns

ALICE FAKT

Department of Environmental and Energy Sciences

CHALMERS UNIVERSITY OF TECHNOLOGY

Gothenburg, Sweden 2026

Towards electrified cement production
Modelling studies of heat transfer conditions in plasma-heated rotary kilns

ALICE FAKT

Department of Environmental and Energy Sciences
Chalmers University of Technology
SE-412 96 Gothenburg
Sweden

Printed by Chalmers Reproservice
Gothenburg, Sweden 2026

Towards electrified cement production

Modelling studies of heat transfer conditions in plasma-heated rotary kilns

ALICE FAKT
Division of Energy Technology
Department of Environmental and Energy Sciences
Chalmers University of Technology

Abstract

Fossil fuel combustion is the dominant heat source in energy-intensive industries, why electrification of these industries is essential for mitigating global warming. A major challenge is the electrification of the cement industry rotary-kiln heat-treatment process, which has a high energy demand and requires high temperatures. Thermal plasma technology presents a suitable alternative for electrifying the rotary kiln. Plasma torches use electricity to produce a high-enthalpy gas plume, capable of providing high temperature conditions. However, a change from conventional burners to plasma torches entails a change in the complex heat transfer conditions governing the rotary kiln process.

The heat transfer in combustion-based rotary kilns is dominated by radiative heat transfer, with particle radiation from soot, ash and fuel particles being a major contributor. Hence, the lack of suspended particles in the plasma heated gas poses a challenge for the implementation in rotary kiln. Further, high peak temperatures near the torch expose the kiln refractory to new temperature conditions. To facilitate implementation of plasma torches in industrial kilns, modeling and experimental work on pilot- and demonstration scale is needed.

This thesis concerns modelling of a pilot-scale plasma-heated kiln, simulating industrial conditions. The work assesses heat transfer conditions in plasma-heated rotary kilns to identify how operational conditions may be adjusted to ensure sufficient heat transfer from the gas domain to the bed material. Potential issues, such as overheating of the wall and impact on the regenerative heat transfer, when implementing plasma heating are also assessed. Within this work, two models are employed: a three-dimensional kiln heat transfer model that obtains details on the heat transfer conditions and temperatures of the surfaces in plasma-heated kilns, including a moving product bed, incorporating plasma torch measurement data to estimate the gas temperature profile. The second model applies a one-dimensional conduction model that is developed and coupled to the kiln model to assess the radial and angular temperature distribution within the rotating wall.

By adapting operational parameters like directing the plasma torch towards the bed, increasing bed feed rate, and particle injection, this thesis concludes on the potential for plasma torches as the heat source in cement rotary kilns. While particle injection and tilting of the plasma torch is shown to achieve sufficient heat transfer conditions for producing cement clinker, potential overheating of the wall may be mitigated by increasing shell cooling and bed feed rate.

Keywords: Heat transfer, cement, rotary kilns, thermal plasma

List of publications

The thesis is based on the following appended papers, which are referred to in the text by their assigned Roman numerals:

I. A. Fakt, A. Gunnarsson, K. Andersson, F. Normann, and B. Wilhelmsson, "Evaluating Heat Transfer Conditions in a Plasma-Heated Rotary Kiln for Cement Production " *Ind. Eng. Chem. Res.,* vol. 64, no. 16, pp. 7491-8542, 2025 "Evaluating Heat Transfer Conditions in a Plasma-Heated Rotary Kiln for Cement Production " *Ind. Eng. Chem. Res.,* vol. 64, no. 16, pp. 7491-8542, 2025, https://doi.org/10.1021/acs.iecr.

II. A. Fakt, A. Gunnarsson, K. Andersson, F. Normann. "Modelling approaches to assess wall temperature conditions and cyclic temperature variation in a plasma-heated rotary kiln". In manuscript.

Alice Fakt is the main author of **Papers I-II,** and performed the modelling, method development and analysis for both papers. Assistant Professor Adrian Gunnarsson has contributed with method and model development and modelling resources (3D heat transfer tool), discussions, writing and editing. Professor Fredrik Normann and Professor Klas Andersson have contributed with discussions, method development, writing and editing. Dr. Bodil Wilhelmsson has contributed with discussions and editing of Paper I.

Acknowledgments

Without the people around me, this work would consist of only blank pages. I wish that I could express my gratitude to every one of you, but one page would not be enough so I will keep it short. I will start with my supervisors, Klas Andersson, Fredrik Normann, and Adrian Gunnarsson. I am grateful for all the time and effort you put in to push me and this work forward, for your constant support and for keeping me motivated. From every discussion, I take with me new perspectives and ideas. Adrian, thank you for always checking in, for double- and triple checking whenever I need it, and for your constant encouragement and support.

To the High temperature process group, thank you for creating a space for curiosity, feedback, and endless discussions. I keep learning from all of you. Elias and Ibrahim, thank you for all the discussions on heat transfer, kilns, plasma and modelling. You keep me inspired and curious! I also wish to express my gratitude to Bodil Wilhelmsson at Heidelberg Materials, for discussions and input, and providing me with a valuable industry perspective.

To my friends in the division, thank you for making me laugh every day. Thank you for all the stupid lunch topics, coffee breaks, Friday fika, fika on other days, ice cream in the sun, going for snacks, running around Mossen, betting on GVFÖ, beer at Pripps… The list is long, yes most of it is related to snacks, and yes all of it has directly contributed to this thesis.

Finally, to the people outside of this office: to my family and my friends. For all the laughter, for your endless support, for being there to celebrate the victories and bring me back from defeats, for reminding me that *it's not that deep*. I would not be able to do this without you, ni är bäst!

Alice Fakt
Göteborg, Sweden
May, 2026

Table of Contents

Outline

This thesis consists of six chapters, providing a summary of the work and two appended papers. Chapter 1 introduces the motivation of this work and the aim and scope of the thesis. The background and theory related to this thesis, including previous research within the field, is covered in Chapter 2. Chapter 3 summarizes the overall method of the thesis, and the modelling approaches used in the two appended papers. In Chapter 4, selected results are presented and discussed, concluding and presenting directions for future work in Chapters 5 and 6, respectively.

Paper I assesses the heat transfer conditions from a plasma-heated CO_2 gas in an $8MW_{el}$ demonstration kiln for cement production, using a 3D rotary kiln heat transfer model. The model implements a plasma temperature profile up-scaled based on measurements on a $50kW_{el}$ CO_2 plasma torch. The study evaluates the impact of kiln dimensions and operating conditions on the heat transfer from the plasma-heated gas to the bed material, identifying approaches to enhance the heat transfer conditions within the kiln.

Paper II focuses on the cyclic heat transfer within the kiln wall, and between the bed and wall, employing a finite difference methodology to solve for the time-dependent temperature profile in the wall of a pilot scale kiln. The effect of an asymetrical gas temperature profile, shell cooling, and bed feed rate on the thermal load of the wall is assessed.

1 Introduction

The Paris agreement states that the global temperature increase should be limited to 1.5°C above pre-industrial level to mitigate global warming caused by human activities [1]. Energy intensive industries such as the cement, iron, and petrochemical sector account for about a quarter of CO_2 emissions globally, hence decarbonization of these industries is key for reaching the targets of the Paris agreement. The cement sector alone is responsible for up to 7% of global CO_2 emissions, generating approximately one ton of CO_2 per ton of produced cement [2]. During the past 20 years, the European cement production has been steadily increasing, with a production of 165 million ton cement in 2020 [3]. Decarbonization of the cement industry poses a major challenge due to the high-temperature heat requirements in the process, where electrification through the use of plasma torches is one option to provide heat to the process [4].

To produce Portland cement, mined raw material mainly consisting of limestone, undergoes a series of heating steps. A central step in the production of cement is the calcination reaction, where CO_2 is released from the limestone as it is heated. Approximately 60% of the associated emissions originate from the calcination. The remaining emissions are related to the combustion of fuels to supply heat for the calcination and following clinker reactions. Due to the high temperatures required for the raw material to undergo the fundamental reactions, coal is widely used as the main fuel in the process. The largest unit which also requires the highest temperatures is the rotary kiln, where the product needs to reach 1450°C [5]. Transitioning from fossil fueled systems to electrified systems entails a challenge in achieving sufficient heat transfer that can provide similar conditions in the kiln for the bed material to undergo the necessary stages to produce clinker. Conventional electric heating methods like induction heating and resistive heating elements are restricted to lower temperatures due to material constraints and are hence not suitable for clinkerisation. Instead, plasma torches are shown to be a promising electric heat source, producing a high-temperature, flame-like plasma-heated gas [4].

Different gases can be used as plasma forming gas, however one of the most attractive options for cement rotary kilns is to use CO_2. As CO_2 is inherently formed during limestone calcination, it is already available at the plant and is chemically compatible with the cement process. Further advantages of substituting combustion with plasma torch technology include elimination of NO_x formation, under the assumption that a gas tight process with no false air can be achieved, and flue gases from the process will have a high CO_2 concentration, providing advantageous technical and economic conditions for carbon capture [4].

A core difference between a flame produced by fuel combustion and plasma-heated gas is the presence of suspended particles. Direct fired rotary kilns are strongly dominated by the radiative heat transfer, and while plasma torches are shown to hold high temperatures, they are also characterized by a short, highly radiative zone near the torch. Further downstream from the torch, the plasma-heated gas transitions to a convection dominated zone [6]. These features cause new heat transfer conditions to be accounted for when retrofitting existing rotary kilns, or designing new kilns, in the transition from fuel burners to plasma torches. High temperature

zones near the torch, and a reduced radiative contribution towards the bed material inlet can cause large temperature distributions in the kiln wall, conditions which traditional kilns are not necessarily designed to withstand. Industrial kilns are also under high mechanical load, making them sensitive to thermal deformation. Predicting possible heat transfer conditions and the resulting wall and bed material temperatures is of importance for assisting in the transition to electrified kilns, requiring the development of models able to predict the wall temperature conditions.

This thesis aims to contribute to the transition from combustion heating to electrically heated cement rotary kilns by characterizing and quantifying the complex heat exchange between the gas domain, wall, and moving bed. By applying models in both one and three dimensions, the heat transfer conditions in rotary kilns at pilot- and demonstration-scale are examined, finding options to adjust operational parameters to enable favorable conditions for producing cement clinker with a plasma torch as the heat source.

1.1 Aim and scope

The over-arching aim of this thesis is to assess the heat transfer conditions in plasma-heated cement rotary kilns, indicating possible advantages and challenges when implementing a plasma torch in a rotary kiln and how to mitigate potential issues. The motivation lies in the cement industry's need to reduce CO_2 emissions, specifically targeting energy related emissions. To facilitate implementation of plasma on industrial scale, it is necessary to first model and evaluate conditions in smaller scale kilns. Hence, this work aims to assess the heat transfer conditions in a smaller pilot-scale kiln, and a larger demonstration-scale kiln replicating the operational and geometrical conditions of an industrial kiln. This works contributes to the field by characterizing the heat transfer conditions in rotary kilns operating with plasma as a heat source, indicating heat transfer enhancement options, and wall temperature behavior. This thesis aims to:

- Evaluate the heat transfer conditions in plasma-heated rotary kilns by quantifying relative contributions from radiation, convection, and conduction to the solid bed
- Identify how operational conditions of the kiln and plasma torch can be modified to ensure sufficient heat transfer to the bed, and the impact of changing dimensional and operational parameters
- Evaluate the cyclic wall temperature fluctuation and the effect of asymmetric gas temperature profile and shell cooling

As the unit with the highest thermal energy demand in the cement production process, this study is centered around the heat transfer conditions and resulting temperature distribution in the rotary kiln. One kiln at demonstration scale, simulating industrial conditions, and one pilot-scale kiln is modeled. Heat released and absorbed by reactions in the bed is accounted for, but reaction mechanisms are not modelled. The scope of this thesis is limited to the rotary kiln itself, excluding heat recovery of the flue gases leaving the kiln and the impact on mass and heat balances of the process steps up- and downstream of the kiln. Future work aims to expand the scope to include evaluation of the impact on process parameters of the preheating steps, calcination, and cooler when transitioning from combustion to plasma heating.

2 Background

The theoretical background and related research are covered in this chapter. First, an overview of the cement production process and possible options for reducing emissions related to the process is presented, followed by a general description of plasma torches for industrial applications. The second half concerns heat transfer in rotary kilns, and relevant approaches applied in rotary kiln modelling.

2.1 The cement process

Production of cement starts with extraction of raw materials, mainly limestone, which are transported to the plant. The raw material is crushed and milled together with additives to a desired composition. The material is then ground to a fine meal, known as raw meal, where limestone constitutes around 80wt% of the raw meal mixture. Figure 1 illustrates the heat treatment steps, including preheater cyclones, calciner, rotary kiln, and cooler. The blue solid lines represent the direction of the solids, and the orange dashed line the gas flow direction. The meal is preheated in a preheater tower, consisting of a series of cyclones, where thermal energy is recovered by utilizing hot exhaust gases from the downstream rotary kiln and calciner to preheat the meal. At the bottom of the preheater tower, a combustion chamber known as the calciner is located, where a majority of the meal is calcined and carbon dioxide is inherently released from the limestone as shown by the calcination reaction presented in R1. Approximately 40% of the thermal energy supplied to the plant is supplied to the calciner through combustion [4].

$$CaCO_3 + heat \rightarrow CaO + CO_2 \qquad \text{R1}$$

The calcined meal enters the rotary kiln at ~900°C. The rotary kiln is typically 60-80m long, with a diameter of 2-4m. As the kiln is tilted and continuously rotating, the raw meal is transported downwards through the kiln towards the flame, where fuel is added to ensure temperatures are sufficient for sintering of the material at around 1450°C. At the end of the kiln, cement clinker is formed which is cooled rapidly to ensure stability of the formed materials. The clinker is cooled using large amounts of air, and the air leaving the cooler at around 1000°C is re-used as secondary air in the kiln, and tertiary air in the calciner. Lastly, the clinker is ground to a fine meal together with gypsum and other additives [4].

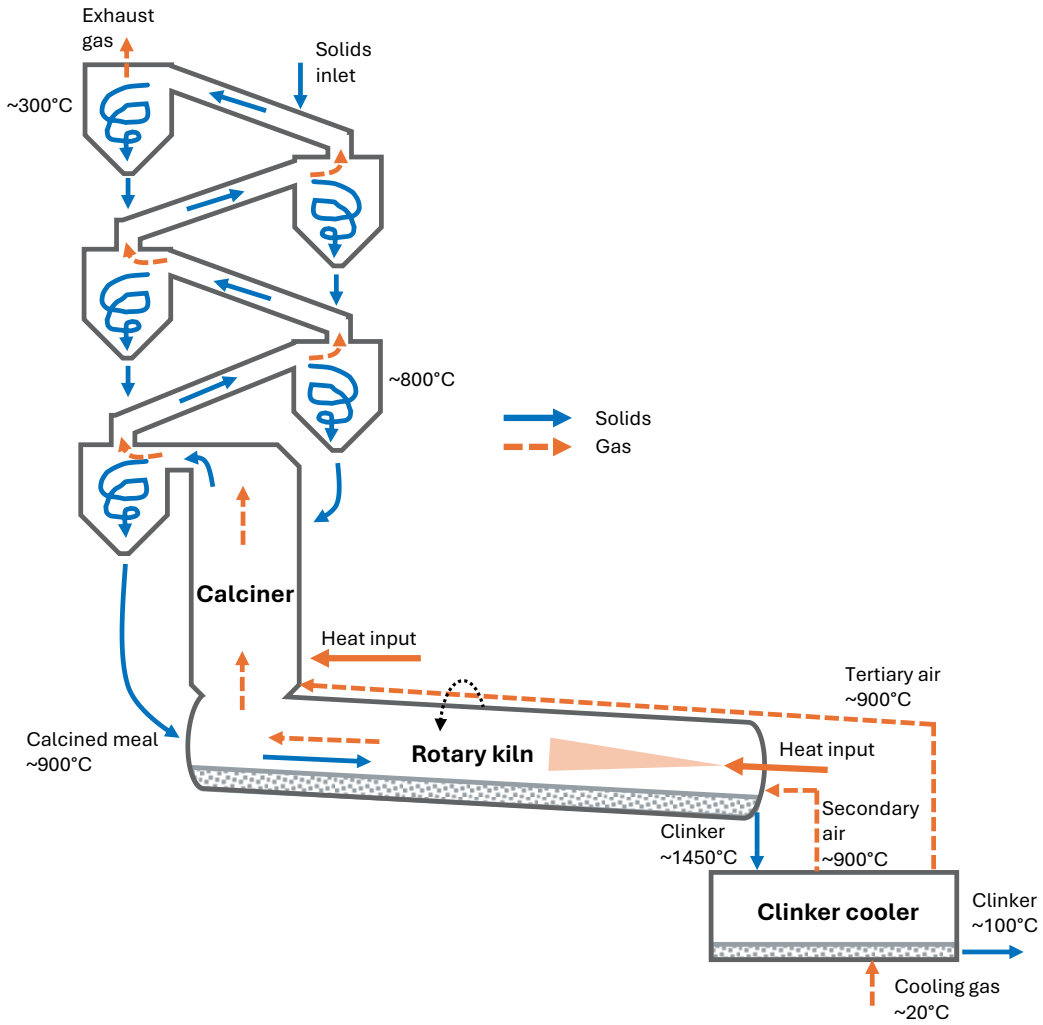

Figure 1. Schematic of the cement process, including temperatures of the gas and solids entering and leaving each unit.

2.1.1 Preheater systems

Modern plants are today equipped with suspension preheaters and a calciner, known as preheater-precalciner systems. In these systems, the meal is almost fully calcined as it enters the rotary kiln, allowing for shorter kilns to be used [5].

The preheating system consists of a series of cyclones, typically between four to six cyclone stages, arranged on top of each other in a tower. The raw meal is fed at the top, right before the uppermost cyclone, where it is mixed with the exhaust gases as it enters the cyclone. In each cyclone, the raw meal particles are separated from the gas as it leaves at the bottom and is again mixed with the gas from the cyclone underneath. This is repeated at each cyclone stage, alternatively mixing and separating the gas and solids. Figure 2 illustrates the mixing and separation of the gas and solids stream in a cyclone stage. The temperature is gradually increased for each stage, the top cyclone having the lowest temperature (~300°C) to the bottom cyclone at the highest (~800°C). The repeated mixing and separating, in combination with large contact surface area between the gas and solids at increasing temperature stages ensures optimal heat transfer. Flue gases from the rotary kiln are fed to the bottom cyclone, and moves

upwards through the stages [5]. In the preheater system, the temperature of the raw meal is increased from around 60°C to ~860°C, and the temperature of the flue gases from the kiln is reduced from ~1100°C to ~350°C as it leaves the top cyclone [4].

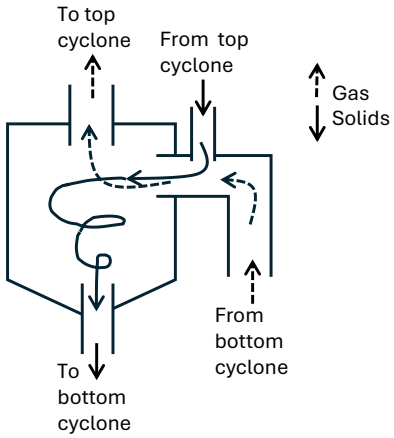

Figure 2. Schematic of mixing and separation of solids and gas in a cyclone, the gas stream supplied from the cyclone stage underneath and mixed with the solids from the upper cyclone.

From the bottom cyclone, the meal is fed to a calciner. The calciner is a large combustion chamber where supplementary firing occurs. Preheated air from the cooler bypasses the kiln and is used as primary air for the combustion in the calciner, hence the efficiency of the pre-calciner systems is strongly linked to the cooler design. Some calcination occurs in the cyclones prior to the calciner, however the majority of the heat supplied to the calciner is used to calcine the meal, achieving up to 95% calcination degree before entering the rotary kiln [5]. Operational parameters influencing the calcination degree in the calciner include the residence time of the raw meal, gas/solids separation, temperature, and dust circulation. Systems with shorter solids residence times show wide fluctuations in the degree of calcination. Preheater-precalciner systems aim to reduce the heat demand in the rotary kiln, achieve a controllable degree of calcination, as well as abate NO_x emissions through use of alternative fuels [7].

2.1.2 Rotary kilns for cement production

Rotary kilns are used by multiple types of industries for material processing, including iron ore pelletization, hazardous waste reclamation and cement clinker production. This widespread use is attributed to their ability to handle a variety of materials with large variations in particle size and to their ability to maintain specific environments. Rotary kilns operate as large counter current heat exchangers, exchanging heat between the hot gas phase and the passing bed material, allowing direct contact between the freeboard gas and the solid bed [8].

Most common in cement industry today is to use dry kilns, equipped with a preheater-precalciner tower. The solids residence time in dry kilns equipped with preheater-precalciner tower is typically around 20 minutes, while the residence time in the preheater towers itself is around a minute [9]. The dry kiln is typically divided into four zones: the calcining zone (805-1200°C), the upper-transition zone (1200-1400°C), the sintering zone (1400-1510°C), and the cooling zone (1510-1290°C). Commonly, the upper transition zone and the sintering zone are referred to together as the burning zone. In the upper-transition zone, the main reactions in the bed are mostly a continuation of the calcination, and initial formation of belite (C_2S), which

continues into the sintering zone. The sintering reaction requires high temperatures, where formation of alite (C_3S) is the central reaction [10]. There is also significant formation of liquid phase in the sintering zone, allowing clinker mineral formation to occur more rapidly [9]. The final few meters of the kiln before the discharge is referred to as the cooling zone, where the temperature of the clinker is reduced to around 1300°C before rapid cooling in the cooler to ensure stability of the formed minerals, preventing the reversion of alite to belite [9, 10].

The bed motion can be categorized into two components, movement in the axial direction which is the main influence on the residence time, and transverse movement, influencing heat transfer rate and material mixing. Figure 3 illustrates the axial counter-current flow of the gas and solid bed in the kiln, and the transverse bed motion with the bottom bed layer moving with the wall and the top layer moving downwards. The transverse bed motion is determined by the rotational speed of the kiln, typically categorized into six different modes: slipping, slumping rolling, cascading, cataracting, and centrifuging, where centrifuging occurs at high rotational speeds and slipping at low speeds [8]. Rolling bed motion is the preferred mode, providing optimal heat transfer conditions due to good mixing. For rolling bed motion, the dynamic angle of repose, defined as the angle of the bed surface to the horizontal, is near constant throughout the kiln, achieving a somewhat even axial bed height [11]. The filling degree is one of the major factors influencing the heat transfer process, relating to the heat transfer area [12].

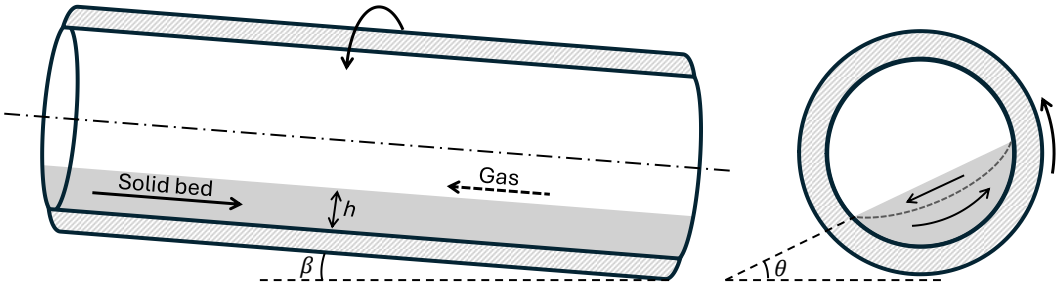

Figure 3. Axial motion and counter-current flow of the bed and solids (left) and transverse solid motion (right), defining bed height h, dynamic angle of repose θ, and kiln inclination β.

The geometry and operational settings of a rotary kiln determine the solids axial and transverse transport, directly impacting the solids residence time, mixing, and heat transfer characteristics of the solid bed. Characteristics of the solids transverse and axial motion has been researched by many [13-15], including efforts to predict the mean residence time of the solid bed [16-18]. The main operational parameters affecting the solids transport are the material feed rate, kiln inclination, and rotational speed of the kiln, along with the kiln geometry, specifically the inner diameter and length of the kiln. For a fixed kiln inclination, an increased rotational speed will reduce the average filling degree of the kiln, reducing the solids residence time. Similarly, increasing the kiln inclination while keeping the rotational speed constant reduces the residence time [19]. When only the feed rate is increased, the residence time is reduced while the kiln hold-up is increased, the effect is however marginal for kilns without an exit dam. Increased filling degree due to increased feed rate results in a reduction in residence time, while an increase in filling degree caused by changes in rotational speed or inclination of the kiln instead

increases the residence time. The residence time is also increased with increasing inner diameter and kiln length [20].

Fuel is introduced to the kiln via the main burner on a lance at the bottom end. The burner produces a flame with temperatures of around 2000°C, and the flame is adjusted by the primary air supply. Coal is the most widely used fuel in cement kilns, with oil and natural gas also commonly used globally. For combustion of solid fuels, particle size highly influences the rate of combustion, with smaller particles being heated at a faster rate, resulting in higher peak temperatures essential for achieving clinker formation. High temperature combustion air is required to ensure rapid combustion, hence secondary air from the cooler is mixed with ambient temperature air and the finely ground coal to achieve sufficient momentum [21]. The flame temperature in the kiln depends on the rate of fuel/air mixing, coal particle size, fuel moisture content, temperature of the combustion air, and the amount of excess air in the process. Excess air is allowed in the system to ensure complete combustion but also includes some false air entering the process due to improper sealing. Insufficient mixing, large fuel particles or high moisture content results in incomplete combustion, and the formation of ash and carbon monoxide [7]. In direct fired kilns, ash from the solid fuel will be incorporated into the cement clinker, which needs to be accounted for in the raw material composition [21]. Alternative fuels of both fossil and biogenic origins are used in cement manufacturing today. Some alternative fuels of fossil origin include used tires, plastics, and waste oil, and of biogenic origin include agricultural waste and waste-water sludge. Refuse derived fuel (RDF) comprises a large fraction of alternative fuels used in German cement plants. Challenges related to combustion of alternative fuels include fuel composition, moisture content, and particle size. Minor elements in alternative fuels are mixed with the clinker and can have a significant impact on process stability and clinker reactivity, and high content of chlorine causes corrosion of steel reinforcements in the final concrete. High moisture contents prevent fine milling during preparation of the fuels, resulting in larger particle sizes that cause longer combustion time. Hence, alternative fuels are more suitable for substitution in the calciner rather than in the kiln [22].

Rotary kilns used for cement production are prone to the formation of a coating layer on the inner wall, which occurs as the material solidifies from a liquid- or semi-liquid state. Coating formation continues as long as the temperature of the coating surface is below the solidifying temperature of the clinker bed, as the temperature at the coating surface exceeds solidifying temperature the particles continues to melt and the coating continues to grow. However, when the kiln is operating at stable conditions the coating is self-maintained and no new coating is formed. As the surface temperature of the refractory is one of the most influential parameters affecting the coating, the heat transfer from the heat source plays a significant role in the formation of the coating layer [10]. Refractory materials used for rotary kiln must be able to withstand various types of compressive and tensile stresses, at extreme temperatures. Mechanical stress in the wall caused by temperature gradients in the refractory deforms and reduces the load-bearing capacity of the kiln refractory. Some factors influencing the refractory life include operational changes, unstable flame conditions, and temperature cycling, all of which can cause cracking and erosion of the refractory [23].

2.1.3 Clinker cooler

The clinker cooler serves dual purpose: reducing the clinker temperature to ensure good quality of the clinker phases, and to recover heat to be used as secondary and tertiary air for combustion in the rotary kiln and calciner. The clinker is cooled to around 1200°C during the final few meters of the kiln, before entering the cooler. A wide variety of coolers are used in cement manufacturing today, categorized into tube coolers (rotary or planetary), grate coolers (traveling or reciprocating), and gravity coolers (shaft or vertical) [5].

Rotary coolers use the same principle as the rotary kiln but for reverse heat exchange, rotational speed and internal lifters influence the performance of the cooler. Planetary coolers consist of several cooling tubes attached at the discharge end of the kiln. It is not possible to efficiently extract tertiary air in planetary coolers, making them incompatible with precalciner systems. In travelling grate coolers, the clinker bed is transported on a moving grate, with cold air blown in a crossflow from under the bed grate. Reciprocating grate coolers work by stepwise pushing the clinker bed [5]. Grate coolers have a high heat transfer contact area, ensuring fast cooling. Grate coolers also allow for high clinker capacities, making the grate cooler the preferred system in modern plants. In gravity coolers cooling air never comes in contact with the clinker, as the clinker descends over steel tubes cooled by air flowing through them. It has been shown in practice that there is no significant difference in the clinker quality between the different cooler types, instead the choice of grate design is more important for recovering heat from the hot clinker. The rate of clinker discharge from the kiln may vary greatly for kilns prone to coating and ring formation. An advantage of the rotary cooler is that the movement of clinker can be controlled independent of the kiln discharge rate. Slow cooling in the kiln to around 1200°C followed by rapid cooling to around 100°C maximizes the formation of alite and stabilizes belite phases [7].

2.2 Emission reduction options for the cement process

Around 60% of the emissions in the cement industry originate from the calcination reaction, and the remaining 40% are fuel related emissions [4]. As of 2023, around 60% of the energy supplied to Swedish cement plants comes from alternative fuels [24]. To reduce emissions from the cement industry, multiple decarbonization strategies are currently explored, targeting both the fuel and process related emissions. Three main CO_2 mitigation paths are identified:

- Implementation of carbon capture technologies
- Reduction of process emissions from calcination by using alternative raw materials and cement compositions
- Reduction of fuel emissions for thermal processes through kiln electrification and/or use of alternative fuels

The International Energy Agency (IEA) states that carbon capture utilization and storage (CCUS) will play the main role in reducing emissions from cement industry [25]. Due to the inherent release of CO_2 during limestone calcination, flue gases from the cement industry contain high CO_2 concentrations, strengthening the case for CCS. Carbon capture systems can generally be categorized as: post-combustion and pre-combustion capture. Post-combustion capture refers to CO_2 captured from flue gases produced by combustion of fossil- or bio-based

fuels. Pre-combustion technologies involve reacting the fuel with air or steam to produce syngas, composed of mainly CO and H_2. Flue gases from cement production contain around 15-30vol%, making post-combustion capture a suitable technology. Separation of CO_2 from the flue gases is achieved by a chemical absorbent. The chemical absorbent then releases the CO_2 after being heated and can be recycled for continued absorption. Implementation of post-combustion carbon capture in cement plants will however require additional steam generation to regenerate the solvent. Additional energy is also required to compress the captured CO_2 to enable transport and storage [26]. The world's first cement carbon-capture facility was recently opened in Brevik, Norway, in June 2025, using an amine-based post-combustion capture system [27].

Reduction of the calcination-related process emissions can be achieved by substituting a part of the clinker with alternative raw materials. For Portland cement, it is possible to replace some of the clinker constituents with materials known as supplementary cementitious materials (SCM). Some SCMs include granulated blast furnace slag, fly ash, and pozzolanas. As these materials partially replace clinker constituents, both energy related and process related emissions are reduced [3]. Currently, up to 20% of the clinker produced by Heidelberg Materials Cement Sverige is substituted with blast furnace slag and fly ashes [24].

Actions for reducing fuel related emissions include substitution of the currently used fossil fuel by carbon neutral fuels such as biomass or waste, or transitioning from combustion by electrifying the process. Cement rotary kilns are fuel flexible and can burn both waste derived fuels and biomass. For economic reasons, biomass supply is focused on waste streams rather than biofuels. However, the waste quality should be suitable for co-processing, thus high moisture content, and high percentage of chlorine and heavy metals are not acceptable due to deterioration of the kiln and trace elements impacting the clinker quality. Electrification options for providing process heat include plasma, microwave heating, induction heating, and resistive electrical heating [3]. A feasibility study performed within the CemZero project investigated electric heating of a pilot scale rotary kiln, successfully concluding on the possibility of using plasma torches or resistive heating elements (for calcination) as the heat source in a pilot scale rotary kiln [4].

Some recent projects focusing on electrification of either the calcination step or clinkerization include projects like LEILAC, Decarbonate, ELSE, CemZero, and ELECTRA. Within the LEILAC project, an electrified direct separation reactor was developed to separate and capture the CO_2 as it is released during limestone calcination. The unit is designed to be fuel flexible, using heat sources such as hydrogen, biomass, or electricity [28]. The Decarbonate project analyzed limestone calcination in an electrically heated rotary kiln, using resistive heating elements. Raw meal for cement production was successfully treated to fully calcined meal, with similar qualities to that achieved in a traditional calciner [29]. Another project focusing on electrifying the calcination step is the ELSE project. Process modelling in Aspen Plus comparing a coal fired calciner to an electrified calciner showed a reduced clinker production due to the reduced ash content, but a potential reduction of CO_2 emissions of up to 78% for the electrically heated calciner, along with a reduced energy demand if electricity is produced by renewable sources [30]. In the ELECTRA project, a demonstration scale rotary kiln is currently

being developed, using a CO_2 plasma torch as the heat source, enabling efficient CO_2 capture [31].

Figure 4 presents a simplified process diagram of a conceptual design of an electrified process, recirculating the CO_2 stream to two separate plasma generators supplying heat to the calciner and rotary kiln. The concept was proposed in the CemZero project. Due to the calcination of $CaCO_3$, CO_2 is constantly generated in the calciner, and a part of it vented to maintain the mass balance in the system. The CO_2 leaving the preheater system is cooled and filtered before it is used in the plasma generators. The cooler is divided into two sections, the first section uses CO_2 to cool the clinker, followed by a section using air for cooling, the two sections are separated to prevent air leakage into the process. A major advantage of this concept is the possibility to achieve 100% capture of the generated CO_2 leaving the process, as the CO_2 is never mixed with air [4].

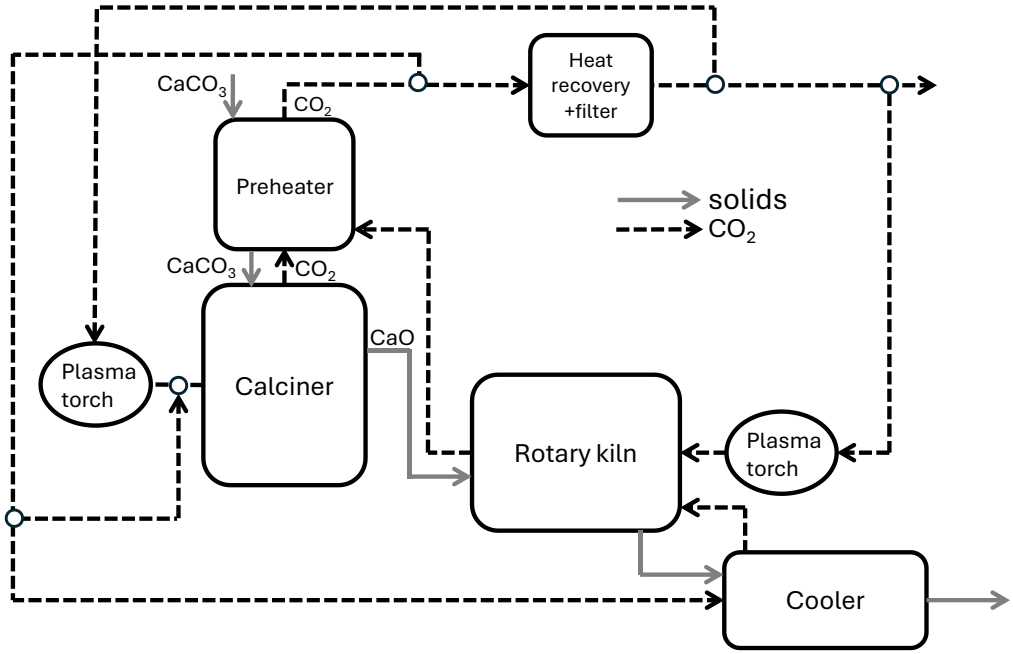

Figure 4. Simplified process flow chart for showing the closed-loop CO_2 recirculation for a conceptual design of an electrified rotary kiln and calciner process, dashed line showing the flow of CO_2, and solid grey lines the flow of solids, interpreted from [4].

A techno-economic assessment of four electrified Portland cement plant concepts, one fully electrified case and two partially electrified cases, based on concepts developed in the CemZero project, was carried out by Quevedo Parra et al. [32]. In the fully electrified case, the heat demand in the calciner is met through resistive heating elements or magnetic induction, assuming the same degree of calcination as the current reference plant. Air is used as the plasma forming gas, mixed with secondary air from the cooler. The flow of plasma heated gas is controlled to keep clinker outlet temperatures at 1450°C. The first partially electrified case involves oxy-combustion of alternative fuels in the calciner and hydrogen combustion in the rotary kiln. This concept is based on the indirect use of electricity in the rotary kiln through combustion of hydrogen produced via solid oxide electrolysis, utilizing waste heat in the process to produce the required steam. The second partially electrified case consists of an

electrified calciner and a rotary kiln burning alternative fuels, coupled to an MEA based post-combustion capture system. The heat requirement for the CCS unit is assumed to be obtainable in the new plant configuration, capturing 95% of the CO_2 emissions from the rotary kiln. The fully electrified case showed the largest reduction in fuel consumption, followed by the partially electrified case with an electrified calciner combined with alternative fuels in the rotary kiln. For all cases, an increase in heat demand was observed, partly related to the lack of tertiary air to complement the heat demand in the calciner, and partly due to alternative fuels having a lower heating value.

2.3 Plasma torches as heat source

Plasma is commonly referred to as the fourth state of matter, consisting of a mixture of electrons, ions, and neutral particles, thermal plasmas contain only ionized atoms. Thermal plasma can be generated by passing an electrical current through a gas, forming a highly conductive gas. The temperature in the plasma can reach up to orders of 10^3 to 10^4°C, depending on the degree of ionization [33].

Mainly two modes of plasma are used in industrial processes: thermal plasma produced at high pressures, generated using either an electric arc or through microwave heating, and non-equilibrium plasmas generated and low pressures. Thermal plasma torches produce a plasma beam, holding a high temperature, enthalpy and heat flux [34]. A wide range of applications of thermal plasma technologies include coating techniques like plasma spraying, clean melting in metallurgy, and destruction and treatment of hazardous waste materials [35]. There are two types of plasma torches: transferred and non-transferred, the difference being the location of the electrodes. In a non-transferred plasma torch, both the anode and cathode are placed inside the housing, whereas one of the electrodes are located outside of the housing for transferred systems [4].

Common carrier gases used for plasma torches include nitrogen, argon, air, and hydrogen [34]. While carbon dioxide is a less common plasma forming gas, advantages when applied in the cement process include being compatible with process and eliminating the formation of NO_x, under the assumption that no air is present [4]. Within the CemZero project measurements on a CO_2 plasma torch developed by the Swedish company ScanArc Plasma Technologies AB were performed [4]. ScanArc develops DC non-transferred arc plasma torches, with the possibility to implement as heat source in furnaces utilizing CO_2 as the carrier gas. Electrical power inputs of up to 8MW are available, effectively heating the gas to 3000-5000°C [4, 36]. The design consists of a water-cooled anode and cathode, separated by a spacer. A high-voltage high-frequency igniter is used to initiate the arc, which is then stabilized and sustained under a controlled gas flow. A schematic of the plasma torch operating principle is shown in Figure 5, including the water-cooled electrodes separated by a spacer, the gas flow through the torch, and the electric arc. The thermal power output from the plasma torch is regulated by adjusting the current and the gas flow supplied to the torch, with a resulting thermal efficiency around 80-90% [6].

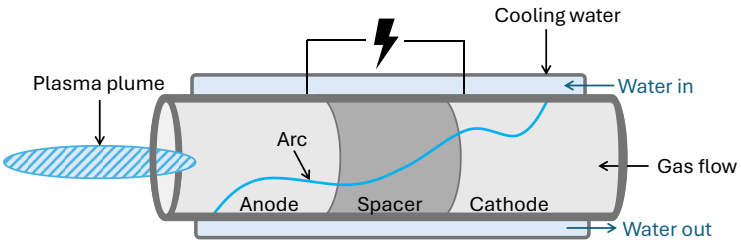

Figure 5. Schematic of the operating principle of a water-cooled plasma torch, the anode and cathode separated by a spacer, based on the torch used in [6]

Plasma torch technology is already widely used for applications such as plasma cutting, welding, and production of high-purity metals [37], but is still not used as the single heat source in continuous high capacity production units. Ko et al. [38] conducted a numerical analysis investigating the heat flow variation in a cement rotary kiln equipped with a coal burner combined with a thermal plasma. For plasma assisted combustion, the gas temperature distribution in the kiln was found to be more uniform compared to conventional combustion. Zaini et al. [39] used a 250kW DC plasma torch in a pilot scale furnace, heating the furnace from ambient temperature to 1200°C using five different plasma forming gas mixtures. Experiments showed a uniform temperature profile within the furnace, with no hot spots, concluding on the potential to heat steel using plasma technology. Amarnath et al. [40] developed a DC non-transferred thermal plasma torch utilizing both CO_2 and CH_4 as plasma forming gases, reaching plasma temperatures of up to 17800K and a thermal efficiency of 73%.

2.4 Rotary kiln heat transfer mechanisms

Figure 6 presents the different modes of heat transfer occurring in the rotary kiln with a bed material, which includes convection and radiation between the gas and solids surfaces, including particles suspended in the gas domain, conduction between and within the bed and wall material, and radiation between the wall and bed. In direct-fired, combustion-heated kilns, radiation is the dominating heat transfer mechanism in the freeboard, constituting around 90% of the total heat transferred from the gas phase to the solids. Convective transfer heat between the gas and solid surfaces occurs due to the turbulent flow of gases. Between the bed and rotating wall, conduction is the main mode of heat transfer, including some radiation in cavities between the wall to the bed. Convective and radiative heat losses occur on the shell of the kiln from heat being conducted through the refractory wall to the outer surface [8].

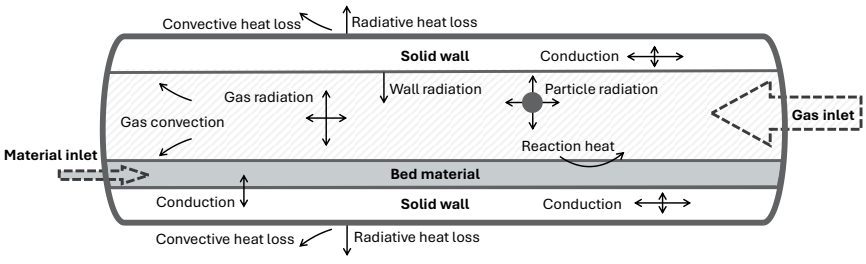

Figure 6. Heat transfer in the axial cross section of the rotary kiln

The thermal performance of the kiln is governed by the complex heat transfer conditions between the gas domain, rotating wall, and solid bed. The relative contribution of each heat

transfer mechanism varies throughout the kiln and depends on flame characteristics and operational conditions. Closer to the burner end of the kiln, thermal radiation is typically the dominant heat transfer mechanism. The radiative contribution increases strongly with temperature, proportional to temperature to the power to four, in accordance with Stefan Boltzmann's law. Incomplete combustion of solid fuels leads to the formation of particles such as soot, ash, and unburnt fuel, being suspended in the gas and contributing to the radiative transfer. These particles may be referred to as broad-band emitters, continuously emitting and absorbing radiation in a wide spectrum, significantly enhancing the radiative heat transfer [41]. Modelling of a full-scale coal-fired iron ore pelletization kiln showed that the overall heat transfer due to radiation is around 81% along the kiln axis, around 10% from convection, and 5% from conduction [42].

Convection occurs due to the motion of the hot gases over the surfaces of the exposed bed and inner wall surface. As the convective heat transfer coefficient is directly linked to the velocity of the gas, the inner geometry of the kiln and operational conditions strongly affect the convective contribution [43]. Tscheng and Watkinson experimentally determined the convective heat transfer coefficient and how it is influenced by gas flow rate, rotational speed and filling degree [12].

Conduction occurs between and within the solid bed and wall. A portion of the transferred heat to the inner surface of the wall is reflected and radiated to the solid bed, and the remaining part is absorbed by the wall. Of the heat absorbed by the wall, some is conducted through the wall to the shell and lost to the surroundings, and the other part is transported with the kiln rotation as the wall passes under the bed, transferring heat into the bed.[44].

Due to the rotation of the kiln, the bed imposes a cyclic temperature change on the wall, cyclically exchanging heat between the wall and bed, commonly referred to as regenerative heat transfer. The wall may hence be divided into two regions: an active inner layer at the inner surface, which is affected by the cyclic temperature change, and a steady state layer not experiencing the temperature variation, as stated by Gorog et al. [45]. The temperature cycling is expected to be the largest at the hotter end of the kiln, or where the temperature difference between the gas and solids is large [45]. Because of this cyclic variation, it is not a steady state heat transfer problem, but a transient process [8].

2.5 Heat transfer modelling

Extensive experimental and modelling work on the heat transfer in rotary kilns using alternative heating technologies has been carried out by our research group at Chalmers University of Technology. Gunnarsson [41] developed and validated a 3D model for simulating the heat transfer conditions in an iron ore kiln heated with coal or oil, and adapted it for cement production. This model was further developed by Ehlmé to simulate the conditions from hydrogen combustion [46, 47] and has been further modified within this thesis for plasma torch heating application. Experimental work characterizing the heat transfer and temperature profiles of plasma torches, and impact of different heat sources and bed material on the heat transfer within a pilot scale rotary kiln was performed by Qasim [6, 48]. Experimental flame characterization of co-firing coal and hydrogen was carried out by Colin, for applications in iron ore kilns [49].

Models of rotary kilns have been developed by many, using different approaches to handle the gas and solids. Mastorakos et al. [50] used a 2D axisymmetric CFD model of the gas domain, coupled to a 1D bed model. Radiation in the kiln was estimated using the Monte-Carlo method, with an explicit finite volume methodology for conduction in the kiln wall. A 3D CFD gas model coupled to a 1D bed model was developed Mujumdar and Ranade [51], applying a P1 radiation model to predict the influence of burner operational parameters. Agrawal and Ghoshdastidar [52] modelled a lime kiln, modelling radiative heat transfer between gas and solids by dividing the wall and bed into surface elements. A stand-alone CFD model was used to determine local conduction coefficients, and a finite difference technique to describe unsteady conduction in the wall. Solids and gas temperature profiles were assumed as well mixed and uniform in the angular direction. Later, this model was further developed by Singh and Ghoshdastidar [53] to include periodic boundary conditions at the inner wall to account for the cyclic temperature variation caused by the bed. Wirtz et al. [54] coupled a 1D radial wall conduction model to a 3D CFD gas model to determine the coating layer profile in a stationary cement rotary kiln, without a bed material. A discrete ordinates method was used to study the radiation, and steady state conduction assumed through the wall to a radiation-convection heat loss boundary at the shell. Pieper et al. [55, 56] further developed the model by coupling a CFD model coupled to a 1D clinker bed model for evaluating the impact of RDF combustion on the coating layer formation with cells blocked-off for the fluid flow to account for the coating layer. A modified discrete ordinates method with radiative properties estimated using a WSGG model is used for radiation calculations, and a penetration model to model the regenerative heat transfer in the wall from the bed.

Efforts to solve the dynamic temperature profile through the wall include the work by Ginsberg and Modigell [57], and Spang [58]. An early 1D dynamic cement kiln model was developed by Spang to evaluate the flame dynamics in the kiln and transient response to changes in gas velocity and kiln speed. Ginsberg and Modigell developed a one-dimensional dynamic rotary kiln model for calcination of titanium dioxide, applying a mixed numerical and analytical approach. Both these models do however neglect the circumferential variation in wall and gas temperature, only considering the radial temperature distribution. A recent model developed by Ryan et al. [59] used a 2D CFD model for the gas domain, coupled to a 1D bed model to predict the onset of calcination and degree of calcination at the outlet in a rotary lime kiln. This model was further developed to study the transient behavior in the kiln, including the dynamic bed temperature and location of the calcination reaction in the kiln [60].

These studies highlight the complex task of developing models that accurately capture the heat transfer mechanisms in rotary kilns, and a lack of models accounting for the transient response of circumferentially asymmetric gas temperature profiles.

Radiation

The radiative transfer equation (RTE) describes the relationship governing the change in radiative intensive at a point along a ray due to emission, absorption and scattering. Exact analytical solutions to the RTE are not possible, requiring methods such as the discrete ordinates method (DOM) to study radiation in rotary kiln. In the DOM, the radiative transfer equation is solved for a set of directions in the 4π solid angle. The radiative heat flux is then obtained by summing all directional intensities weighted by their solid angle fractions [61]. This work employs a DOM, which divides the finite kiln volume into computational cells in

the radial, angular, and axial directions. Properties such as temperature, gas composition, and projected surface area of suspended particles are set at each cell node. In kilns with a present bed material, the bed may be approximated as a flat surface under the assumption of an axially even bed height [42].

Evaluation of the radiative properties of gases, such as absorption coefficients, needs to consider composition, temperature and pressure of the gases present in the gas mixture. One of the most widely used method for gas radiation approximation is the weighted-sum-of-grey-gases (WSGG) model, where gases in the kiln are represented by a mixture of grey gases [61], which is applied in this work.

Convection

Convective heat transfer from the freeboard gas to the exposed surfaces in the kiln are most commonly modelled by applying Newton's cooling law (Equation 1) to determine the heat flux. Newton's cooling law states that the rate of heat transfer between a surface area, A, at temperature T_w and a gas at temperature T_g is proportional to the temperature difference by a coefficient h.

$$Q_{conv} = hA(T_g - T_w) \tag{1}$$

Convective heat transfer coefficients may be obtained empirically through experiments, or theoretically by solving boundary layer equations for the specific geometry [62], for which CFD may be used. Empirical heat transfer coefficients determined by Tscheng and Watkinson [12], Gorog et al. [45] and Barr et al. [63] are commonly applied in rotary kiln models. Applied in this work are convection coefficients from the freeboard gas to solids obtained from Gorog et al., and from Barr et al. for natural convection on the kiln shell.

Conduction

Due to the periodic heating and cooling of the wall from the kiln rotation, the conductive heat transfer through the wall becomes a transient problem. Transient conduction in a one-dimensional cylindrical wall section is described by the Fourier heat equation, expressed in Equation 2.

$$\frac{\partial T}{\partial t} = \frac{k}{\rho C_p}\left(\frac{\partial^2 T}{\partial r^2} + \frac{1}{r}\frac{\partial T}{\partial r}\right) \tag{2}$$

The heat equation describes the temperature change, T, as a function of time, t, and radial position, r, and material constants k, ρ, C_p, corresponding to thermal conductivity, density and heat capacity respectively.

A common analytical approach for solving the transient heat transfer between wall and bed is to apply a penetration model. Wes et al. [64] developed a penetration model for the rotary drum, dividing the wall into an active and a passive layer at the calculated penetration depth. The penetration depth is defined as the distance at which a linearly decreasing temperature would reach a constant value, with the penetration depth increasing with contact time between the bulk materials. At the penetration depth, the rate of change in temperature is near zero. Only

heat conduction in the radial direction is considered, assuming temperature gradients in the tangential and axial direction are small in comparison.

The penetration model is derived from the Fourier heat equation. Applying the boundary conditions BC1 and BC2 yields the error function in presented in Equation 3, where $t_{contact}$ is the contact time between the bed and wall [64].

$$\textbf{BC1}.\ T = T_{surface} \text{ at } r = 0$$

$$\textbf{BC2.}\ T = T_{wall} \text{ at } r = \infty$$

$$dT = \frac{T(r,t) - T_{surface}}{T_{wall} - T_{surface}} = \text{erf}\left(\frac{r}{2} / \sqrt{\frac{kt_{contact}}{\rho C_p}}\right) \tag{3}$$

At the penetration depth, δ, the temperature in the wall approaches the constant value T_{wall}. The temperature distribution over the thermal penetration depth, dT, is set to vary from 0-0.99, in other words the temperature in the wall $T(\delta, t)$ varies from zero up to 99% of the temperature difference between the surface temperature and temperature within the wall. The penetration depth, at $r = \delta$, can then be defined according to Equation 4.

$$\delta = 2\left(\frac{kt_{contact}}{\rho C_p}\right)^{-0.5} * \text{erf}^{-1}(dT) \tag{4}$$

The penetration model developed by Wes et al. was further modified by Schlünder et al. [65], Li et al. [66] and Herz et al. [44, 67]. Experimental studies carried out by Herz et al. measured the contact heat transfer coefficient between the wall and bed in an indirectly heated rotary kiln, and compared with penetration model calculations. They found that the contact heat transfer coefficient increased with a higher rotational speed, larger particle size, and lower filling degree. Further, it was found that the transverse motion of the bed has a significant influence on the contact heat transfer. Sonovane et al. [68] applied a 2D finite element analysis in ANSYS, determining the penetration depth in the wall of a rotary kiln, and evaluated the cyclic wall temperature distribution. At higher rotational speeds and lower filling degree, it was found that the penetration depth and cyclic temperature fluctuation is reduced.

Another approach to solve transient conduction problems is to apply a numerical approach such as the finite difference method. To obtain the finite difference form of Equation 2, the geometry is discretized in both space and time. A forward-difference approximation can be used for the time derivative, as presented in Equation 5. T_n denotes the temperature (T) of each cell node (n) at the previous time (t) and the new time ($t+1$), Δt is the time step size.

$$\frac{\partial T}{\partial t} = \frac{T_n^{t+1} - T_n^t}{\Delta t} \tag{5}$$

A central difference approximation may be used for the spatial derivative, evaluating the temperature in each radial cell, shown in Equation 6. Here, Δr denotes the radial position of each cell.

$$\frac{\partial^2 T}{\partial r^2} = \frac{T_{n-1}^t - T_n^t}{(\Delta r)^2} - \frac{T_n^t - T_{n+1}^t}{(\Delta r)^2} = \frac{T_{n-1}^t - 2T_n^t + T_{n+1}^t}{(\Delta r)^2} \quad (6)$$

The unknown temperatures at time *t+1* can then be determined from known temperature at the previous time *t* by using an explicit solution method, requiring the initial temperature condition at each node. Another solution method is the implicit method, by evaluating all other temperatures at the new time instead of the previous time. To determine the unknown temperatures at the new time, all nodal equations must be solved simultaneously [62].

This work applies both penetration models for the bed and wall, and an explicit finite difference method for conduction through the entire kiln wall.

3 Methods and modelling

In **Paper I**, the heat transfer conditions in a plasma-heated rotary kiln at demonstration-scale were assessed in a three-dimensional kiln heat transfer model, focusing on quantifying the contributions of the heat transfer mechanisms between the plasma-heated gas, wall, and solid bed. Dimensions and gas flows were downscaled to replicate conditions in an industrial scale kiln. Identified was a reduced radiative heat transfer, attributed to the lack of particles suspended in the plasma-heated gas. A set of kiln dimensions was evaluated, finding only a minor improvement on the total heat transfer from the plasma-heated gas to the bed material. Tilting the plasma torch towards the bed as well as introducing particles into the plasma-heated gas was investigated using the model, increasing the heat transfer from the plasma-heated gas to the bed material. Identified in Paper I was locally high temperatures in the wall from tilting the plasma. Thus, in **Paper II**, the wall temperature conditions and the heat transfer interactions between the bed and wall were further assessed by developing a transient one-dimensional model. The cyclic temperature variation in the wall imposed by the bed is investigated for a plasma-heated kiln, along with estimations of the temperatures within the wall. This thesis deals with kilns at two scales: an 8MW demonstration scale replicating industrial scale geometries and gas flow conditions, and a 500kW pilot scale kiln with a smaller length-to-diameter ratio and a thinner refractory lining. Dimensions of the two kilns are based on an industrial kiln and a pilot kiln, both located at Heidelberg Material Cement Sverige's site in Slite.

Figure 7 presents the overall methodology and coupling of the two models. Main inputs and the basis of defining the kiln input are presented on the left-hand side, with relevant outputs from each model presented to the right. The method of upscaling the plasma temperature profile and downscaling kiln dimensions from industrial scale to 8MW demonstration scale is presented in **Paper I** and not further explained in this thesis. The 3D kiln heat transfer model is employed in both papers, while the 1D wall model is developed, applied, and presented in **Paper II**.

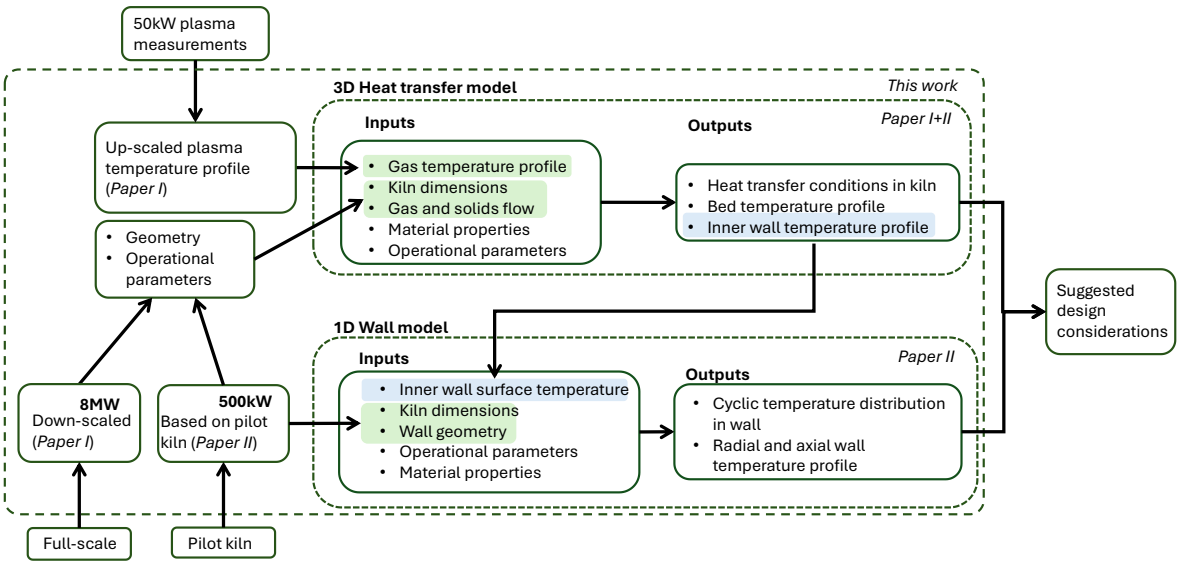

Figure 7. Overall methodology and coupling of the 3D heat transfer model and 1D wall model employed for the two appended papers.

3.1 Models

Two heat transfer models are used to assess the heat transfer within the kiln: a kiln model solving the heat transfer conditions in three dimensions, and a one-dimensional conduction model solving the temperature profile within the kiln wall and how it changes with the kiln rotation. The two models are coupled at the surface of the inner kiln wall, where surface temperatures are calculated in the 3D model and resulting temperatures in the wall determined by the 1D.

3.1.1 3D kiln model

The kiln model employed in this work is a three dimensional heat transfer model, describing the heat transfer conditions within a rotary kiln with a present bed material, a detailed description can be found in Gunnarson et al. [41, 42]. As input, the model requires the temperature profile and composition of the gas domain, along with the geometry and operational parameters of the kiln. To solve the radiative transfer equation, a discrete ordinates method is employed. The kiln is discretized in the radial, axial, and angular direction, each cell holding parameter values of gas and particle temperature, gas concentration, and radiative properties of the gas and solids present. Radiative properties of the gas are estimated using a weighted-sum-of-grey-gases model (WSGGM) [47], using a set of four grey gases and one clear gas to represent the gas mixture in the kiln.

The bed is accounted for as a flat surface partly filling the kiln, characteristic of rolling bed motion. The bed is discretized in the angular direction and divided into two layers: a perfectly mixed top layer and a bottom layer with no mixing. The bottom layer moves with no slip to the wall in the angular direction, and the top layer moves in the opposite direction, falling down along the bed surface. The surface layer is in contact with the gas domain, receiving heat via radiation and convection, as well as some radiation from the wall. The bottom layer is subjected to conduction and radiation from the covered wall. No heat transfer is assumed to occur between the two layers. The axial variation of the bed height is accounted for by approximating an average filling degree using the correlation of Saeman et al. [69], described further in section 3.2.3.

The temperature of the wall in contact with the bed, T_{wb}, is calculated from an energy balance over each angular cell. Equation 7 presents the energy balance of the inner wall surface. Underneath the bed, the hot wall transfer heat to the bed via conduction, $Q_{wb,cond}$ at the contact points, and via radiation, $Q_{wb,rad}$, in gaps between the wall and bed particles. Some of the heat is transferred through the wall due to conduction, $Q_{wb,loss}$, to the outer surface where it is lost to the surroundings.

$$C_{p,w}V_{cell,wb}\rho_w\left(T_{wb} - T_{wb,i}\right) = -(Q_{wb,rad}+Q_{wb,cond} + Q_{wb,loss}) \quad (7)$$

Similarly, the temperature of the wall in contact with the gas, T_{wg}, is determined from a heat balance, where heat is transferred to the wall cell via radiation, $Q_{wg,rad}$, and gas convection, $Q_{wg,conv}$, and removed from the wall by conduction through the wall and lost to the

surroundings, $Q_{wg,loss}$, as expressed in Equation 8. The temperature of the wall in contact with the gas is assumed uniform for each cell, while a temperature gradient over the penetration depth is given from the unsteady-state penetration model for the cells in contact with the bed.

$$C_{p,w}V_{cell,wg}\rho_w(T_{wg}-T_{wg,i}) = Q_{wg,rad}+Q_{wg,conv} - Q_{wg,loss} \quad (8)$$

Here $T_{wb,i}$ and $T_{wg,i}$ are the initial temperatures of the wall cell at the previous angular step in contact with the bed and gas respectively, and ρ_w is the density of the wall material at the inner wall surface. Since the heat transferred to the wall surface is assumed to only partly penetrate the wall, the cell volume receiving the heat is $V_{cell,wg} = A_{cell}\delta_{\psi,max}$ for the wall in contact with the gas, and $V_{cell,wb} = A_{cell}\delta_{\psi}$ underneath the bed, where δ_{ψ} and $\delta_{\psi,max}$ is the penetration depth of each cell. The penetration depth increases with the contact time, hence the volume of the cells affected under the bed increases from first point of contact to the last. The computational cells in the bottom bed layer move in parallel to the wall. When a bed cell has reached the top cell, it is mixed into the surface layer. Similarly, the top layer moves downwards and is mixed into the bottom layer.

The temperature of the bed material in each cell is determined using enthalpy data of a typical raw meal composition in a high CO_2 atmosphere, accounting for the heat released and absorbed due to reactions in the bed. Using the heat transferred from the wall and gas to the bed, the bed temperature in each bed cell is updated. In industrial kilns, almost fully calcined meal enters the rotary kiln, while kilns at demonstration- or pilot-scale may feed raw meal directly to the kiln. If the meal is not calcined, the feed undergoes calcination in the rotary kiln, hence an additional gas flow of carbon dioxide needs to be accounted for. The model checks if the temperature of the bed has exceeded calcination temperature and adds an additional flow of CO_2.

To close the overall energy balance over the kiln, the outlet flue gas temperature is iteratively updated until the heat demand in the kiln equals the thermal input provided by the heat source, as previously described in [46]. The heat balance comprises the heat transferred from the heat source to the bed material, the heat remaining in the gas leaving the kiln, and the surface heat losses. The total gas flow in the kiln is comprised of the plasma forming gas, the CO_2 flow from calcination, and an additional flow of CO_2 at room temperature to account for false air in the kiln.

3.1.2 1D wall model

The 3D kiln model is coupled to a one-dimensional conduction model, solving the transient heat equation for the temperature profile in the kiln wall. A finite difference method is employed to solve the one-dimensional Fourier heat equation in the radial direction. The kiln wall is discretized into radial and angular cells. To account for the rotation of the kiln, each angular cell corresponds to one rotational time step. Using an explicit solution scheme, the radial temperature profile in each angular cell is determined from the temperature profile at the previous angular cell.

The 1D wall model is coupled to the 3D kiln model at the inner wall surface. Accounting for the bed motion and heat transfer to and from the wall from the recurring contact with the bed

and gas. The 3D kiln model is employed to determine the inner wall temperature at each angular position. Two boundary conditions are specified for the 1D wall model, one for the inner wall surface (Equation 9) and for the kiln shell (Equation 10). The temperature at the inner wall surface is calculated by the 3D kiln model (Eqs. 7-8), and for the outer surface of the kiln a heat balance is expressed for the surface transferring heat via radiation and convection to the surroundings.

$$-k\frac{\partial \mathrm{T}}{\partial \mathrm{r}}\Big|_{r=r_i} = T_{w,i} \tag{9}$$

$$-k\frac{\partial \mathrm{T}}{\partial \mathrm{r}}\Big|_{r=r_o} = -h_{o,conv}(T_{ow}^t - T_\infty^t) - \epsilon\sigma\left({T_{ow}^t}^4 - {T_\infty^t}^4\right) \tag{10}$$

At the radial cells in the wall, a finite difference heat equation is expressed as each cell exchanges heat with the adjacent cells. Equation 11 presents the heat balance for the internal cells, where n denotes the present radial cell, $n+1$ the cell one radial step towards the outer wall, and $n-1$ the adjacent cell one step closer to the inside of the kiln. The radial distance from the inner wall surface to the computational cell is denoted r_n.

$$\frac{T_n^{t+1} - T_n^t}{\Delta t} = \frac{k}{\rho C_p}\left(\frac{T_{n+1}^t - 2T_n^t + T_{n-1}^t}{(\Delta r)^2} + \frac{1}{r_n}\frac{T_{n+1}^t - T_{n-1}^t}{2\Delta r}\right) \tag{11}$$

The radial temperature profile is solved for at time $t+1$, given a temperature profile at time t. Hence, an initial temperature profile is required, estimated as a linear temperature decrease from the inner wall temperature at the last wall cell under the bed, to a shell temperature. Figure 8 illustrates the boundary conditions and discretization of the kiln wall in the 1D wall model, the initial temperature profile, $T_{w,i}$, of the wall is defined at $t = 0$, and for $t > 0$ the wall temperature is calculated from the temperature at the previous time step. The initial temperature profile is set as a linear decrease from the inner wall temperature under the top bed cell, obtained from the 3D model, to a guessed value of the outer wall temperature.

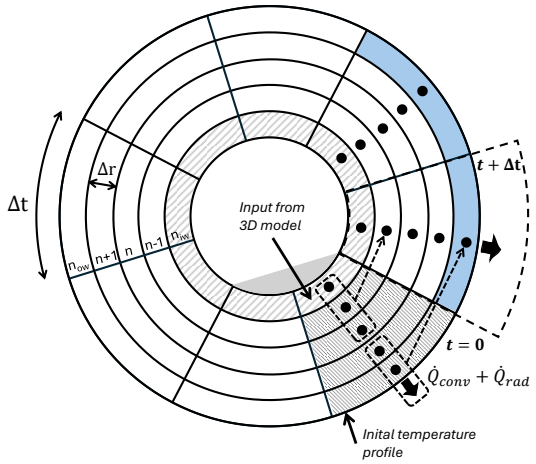

Figure 8. Illustration of the angular and radial discretization of kiln wall, where each time step corresponds to an angular position. Temperatures in all radial nodes from n_{iw} to n_{ow} are determined from the temperatures at the nodes for the previous time step. Dashed arrows illustrate how adjacent boundary cells determine the temperature at $t + \Delta t$, the same methodology is applied for all inner nodes.

3.2 Model inputs

The following sections present the method of determining selected inputs to the 3D model, including estimation of the plasma temperature profile and average bed filling degree determined from operational conditions.

3.2.1 Plasma temperature profile

The model requires a 2D temperature profile of the gas domain, which is then rotated in the 3D model to an axisymmetric temperature profile. Hence, the temperature profile of the plasma-heated gas is approximated as a matrix, each cell containing a value representing the temperature in that position. For this reason, only one half of the temperature profile is required. Further details are given in **Paper I**.

Estimation of the axisymmetric temperature profile is determined by establishing an empirical temperature ratio, relating the axial and radial decrease in temperature from the plasma torch, based on measurements on a 50kW$_{el}$ CO_2 plasma torch [70]. A conical shape of the plasma was observed, and the geometrical constraints are maintained when scaling up the temperature profile to higher heat inputs, assuming constant velocity scaling. The temperature profile of the plasma-heated gas is assumed to be geometrically constrained by the cone and depend on the temperature of the gas surrounding the plasma plume. The plasma is divided into a center line temperature, $T_{c,j}$, and the temperature of the remaining gas in each radial position, $T_{i,j}$. The center line temperature is represented by the first row in the plasma temperature matrix and described by a linear decrease from the peak temperature at the plasma torch to 72% of the peak. Using the temperature ratio expressed in Equation 12, the temperature at each cell, $T_{i,j}$, is calculated.

$$x_{i,j} = \frac{T_{c,j} - T_{i,j}}{T_{c,j} - T_{sur}} \tag{12}$$

Here $x_{i,j}$ is the temperature ratio in each plasma gas cell, determined from measurements on the 50kW$_{el}$ plasma. The peak temperature at the plasma torch is estimated from the enthalpy of CO_2, based on the electrical input and gas flow through the plasma generator. Figure 9 presents the temperature profile of the 50kW$_{el}$ plasma, with labels corresponding to temperature measurements. $T_{c,1} - T_{c,8}$ correspond to the center line, T_{sur} the temperature of the surrounding gas, and $T_{1,1} - T_{9,8}$ the temperature of the plasma plume described by the correlation (Eq 12).

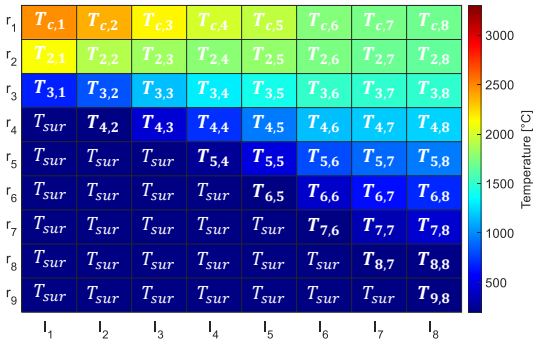

Figure 9. Temperature profile of the 50kW plasma-heated gas, r_9 corresponds to a radius of 0.02m and l_8 a length of 0.14m

3.2.2 Enhancing heat transfer

Modifications are done to the plasma temperature profile to enable tilting of the plasma torch towards the bed, and adding particles in line with the plasma-heated gas. The plasma is tilted by radially displacing the horizontal center line ($T_{c,1} - T_{c,8}$), shifting the entire temperature profile downwards until the center of the plasma meets the bed. Figure 10 displays the axial temperature profile of the gas in the 8MW demonstration kiln. From the axial position where the plasma meets the bed (6m) to the gas outlet at 18m, the temperature profile is linearly interpolated. As the temperature profile is no longe axisymmetric, the top and bottom gas sections are rotated separately to direct the plasma towards the bed.

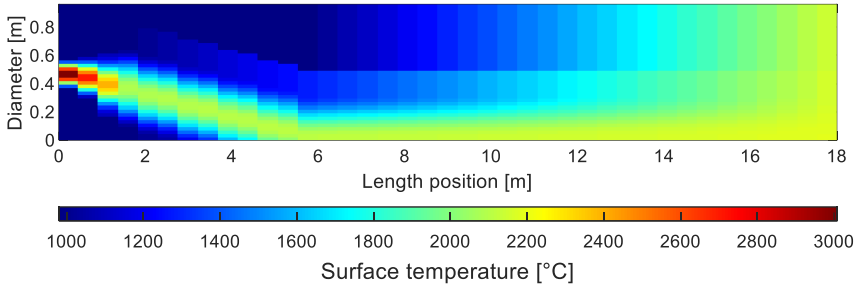

Figure 10. Axial gas temperature profile of the 8MW plasma tilted 5° from the center line. Bed inlet (and gas outlet) at length position 18m and gas inlet (and bed outlet) at length position 0.

Particles are added in line with the conical plasma-heated gas in terms of projected surface area per hour (m^2/h). The particles are assumed as spherical char particles with a radius of 45µm, but a potential option could be to add raw meal particles instead.

3.2.3 Bed motion

The model by Saeman et al. [69] is employed to estimate the axial bed height and hence the filling degree as a function of the bed feed rate, rotational speed, kiln inclination and the kiln geometry. Equation 13 shows the ordinary differential equation describing the axially varying bed height.

$$\frac{dh}{dz} = \frac{3\,\mathrm{TAN}\,\theta}{4\pi\, n}\,\dot{V}(R_i - (h(z) - R_i)^2)^{-\frac{3}{2}} - \frac{\mathrm{TAN}\,\beta}{\mathrm{COS}\,\theta} \tag{13}$$

Where h is the axially (z) varying bed height, θ is the dynamic angle of repose, n the rotational speed of the kiln, $\dot{V}$ the volumetric material feed rate, R_i the inner kiln radius, and β the inclination of the kiln. Dynamic angle of repose is assumed constant and obtained from literature. At the material outlet, a bed height corresponding to a set filling degree is used as the boundary condition to solve the ODE.

The axially varying filling degree is determined from the bed angle, ϵ, according to Equation 14, as done previously [15], and an average filling degree is then calculated which is implemented in the model.

$$FD_z = \frac{\epsilon_z - \sin(\epsilon_z)}{2\pi} \tag{14}$$

Where the local bed angle is determined from the bed height in each axial section according to Equation 15 [16].

$$\epsilon_z = \arccos\left(1 - \frac{h(z)}{R_i}\right) \tag{15}$$

The axial bed motion is accounted for by the axial kiln discretization, treating the kiln as a series of batch reactors, moving a mass of bed from one axial position to the downstream section. The axial residence time in each axial section, t_z, is influenced by the kiln length, L_{kiln}, and the axial speed of the bed, v_{bed}, according to Equation 16.

$$t_z = \frac{L_{kiln}}{n_z v_{bed}} \tag{16}$$

Where the axial bed speed is determined from the cross-sectional area covered by bed, A_{bed}, and the volumetric feed rate, $\dot{m}_{bed}/\rho_{bed}$, described in Equation 17.

$$v_{bed,z} = \frac{\dot{m}_{bed}}{\rho_{bed} A_{bed}} \tag{17}$$

Depending on the number of axial cells used, n_z, each mass of bed will stay in each axial position for t_z seconds. During this time, the kiln completes a number of rotations, n_{rev}, dependent on the angular discretization and rotational speed of the kiln (Equation 18). The angular discretization of the kiln wall, n_ψ, accounts for the transverse motion of the bed. The bed and wall move with an angular speed, $v_{bed,\psi} = 2\pi R_i$, with an angular residence time, t_ψ, in each angular cell, according to Equation 19.

$$n_{rev} = \frac{t_z}{t_\psi n_\psi} = t_z \Omega \tag{18}$$

$$t_\psi = \frac{1}{n_\psi \Omega} \tag{19}$$

3.3 Simulation approach

The modelling work covers two main cases: an $8MW_{el}$ kiln at demonstration scale, and a pilot scale kiln at $500kW_{el}$. Parametrical studies were carried out for both cases, varying geometrical and operational conditions of the two kilns, starting by establishing a base case for each kiln. Geometry and operational conditions of the two reference cases are presented in Table 1. Geometrical dimensions of the demonstration unit were downscaled from an industrial kiln at a reference plant, applying a constant velocity scaling method to determine the inner diameter, and a constant L/D ratio to determine the kiln length, details can be found in **Paper I**. To mimic the conditions in a full-scale kiln, a secondary gas flow is supplied to the kiln, holding a constant temperature of 980°C. The volumetric secondary gas flow in the simulation is set to maintain the same cooling capacity in the cooler as in the industrial kiln, adjusted from air to CO_2. Preheated, fully calcined meal is set to enter the kiln at 900°C. The inclination was not accounted for in the $8MW_{el}$ cases but was added in later versions of the model for estimating the bed height and solids residence time.

The geometry of the pilot scale kiln is based on an experimental kiln, specifications can be found in [48]. Raw meal is fed to the kiln at room temperature, hence the material needs to

undergo both calcination and sintering in the kiln. There is no secondary gas flow, hence the temperature of the gas surrounding the plasma plume is assumed to approach the wall temperature.

Table 1. Geometrical and operational parameters of the reference cases for the two simulated kilns

	Demonstration scale (8MW)	**Pilot scale (500kW)**
Length (m)	18	2.9
Radius (m)	0.48	0.29
Material feed rate (kg/h)	1000 (calcined meal)	300 (raw meal)
Filling degree (%)	10 (constant)	10.54 (average, calculated)
Rotational speed (rpm)	3.8	6
Inclination (°)	-	3
Plasma thermal power (MW)	8	0.5
Plasma gas flow (Nm^3/h)	2285	150

3.3.1 Cyclic temperature variation

As the kiln rotates, the wall is periodically heated by the gas and cooled by the bed, resulting in a cyclic temperature variation. To evaluate the cyclic temperature variation in the wall, the temperature is extracted for an angular cell as it moves with the wall. This is evaluated for each axial section, following one angular cell for all rotations completed for the bed in that axial position. For the pilot scale case with a rotational speed of 6rpm, the wall completes one rotation in 10 seconds. The solids total residence time in the kiln is estimated to 33 minutes (~2000s). With an axial resolution of 42 cells, the bed will stay in one section for 47s. During this time, the wall completes four full rotations, before the bed is moved to the downstream axial section where the wall completes another four rotations. Figure 11 presents an example of the cyclic temperature change for one angular cell at an axial position close to the bed inlet, for the pilot scale kiln at the inner wall surface and at two radial positions in the wall. During all four complete rotations, the wall is heated when in contact with the gas (a-b-c), and the temperature is then reduced when passing under the bed (c-d-e). As the heat is conducted through the wall, similar cyclic behavior occurs in the wall, although at a lower temperature and amplitude.

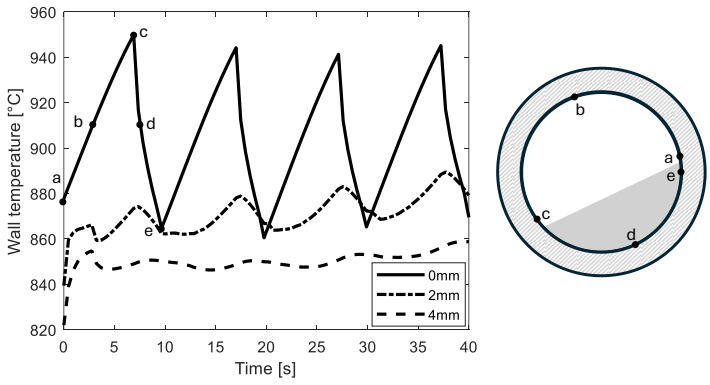

Figure 11. Cyclic temperature variation at the inner wall surface, 2mm into the wall, and 4mm into the wall for the pilot scale case.

4 Selected results and discussion

This chapter presents and discusses the temperature profile of the up-scaled plasma torch, heat transfer conditions and wall temperature distribution for the two cases: demonstration scale at $8MW_{el}$ and pilot scale at $500kW_{el}$. Resulting heat transfer interactions for varying kiln dimensions and operational parameters including feed rate, tilting of plasma and particle injection are presented and discussed. This chapter is divided into two sections: the first section focusing on the modes of heat transfer to the solid bed material, and the second section focusing on the cyclic wall temperature variation caused by the rotation of the kiln and temperature distribution within the kiln wall.

4.1 Heat transfer to bed

Quantifications of the heat transfer mechanisms are presented and discussed in the following section, focusing on the interaction between the plasma-heated gas and the solid bed. Selected results for a variety of kiln dimensions, particle feed rates, and tilting of the plasma are presented.

Kiln dimensions

Impact of kiln dimensions are presented for the $8MW_{el}$ demonstration scale case. The temperatures of the bed and flue gas are presented in 12 for increasing kiln length. For longer kilns, the solids residence time is increased, resulting in an increase in the total heat transfer to the bed. The increased heat transfer to the bed increases the peak temperature of the bed, as well as reduces the flue gas temperature. The shell heat losses rise from the increased surface area of longer kilns, further reducing the flue gas temperature. However, due to the plasma torch producing a short, radiating plume, the peak temperature of the bed is located further away from the bed outlet, as shown by the discrepancy between the outlet bed temperature and peak bed temperature shown in Figure 12. This is not favorable, as the clinker requires rapid and controlled cooling to ensure product quality. As the kiln length exceeds 20m, there is no increase in the bed outlet temperature or reduction in the flue gas temperature, suggesting that increasing the kiln length further will only cause further disagreement between the peak bed temperature and outlet temperature. It is however notable that the material does not reach sufficient temperatures for clinker formation near the bed outlet for any kiln length, requiring other options for increasing the outlet bed temperature. High flue gas temperatures are observed in all cases, further discussion on this may be found in **Paper I**.

Figure 13 presents the heat transfer to the bed for a varying inner radius of the kiln. Total heat transfer refers to the net heat transferred to the bed material. As the cross-section area is increased, the heat transfer area of the bed is increased, resulting in improved radiative and conductive heat transfer. However, gas velocities are reduced when the radius is increased, causing a reduction in the convective contribution. It can be noted that the overall heat transfer to the bed is increased until a breakpoint at a radius of 0.55m where the reduced convection outweighs the increased radiation and conduction, causing an overall reduction in the heat transfer to the bed.

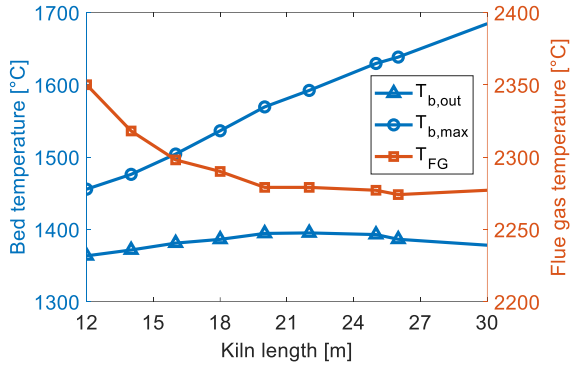

Figure 12. Peak and outlet temperature of the bed material (left axis), and flue gas temperature at the gas outlet (right axis) for the 8MW case.

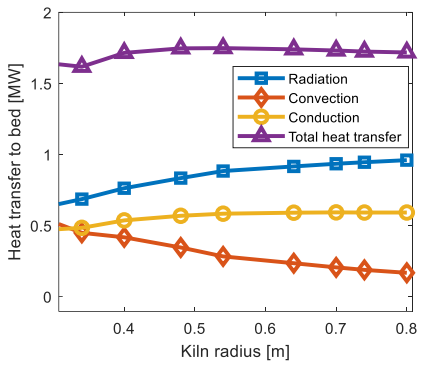

Figure 13. Total heat transfer to the bed and contributions of radiation, convection, and conduction for increasing kiln radius for the 8MW case. Length is kept constant at 18m.

Tilting

Figure 14 presents the heat transfer modes to the bed for increasing plasma tilt angles at $8MW_{el}$. Tilting the plasma towards the bed shows a clear improvement of the total radiative and convective heat transfer from the plasma-heated gas to the bed. Due to the high temperatures in the plasma-heated gas being closer to the bed, the radiative heat transfer is increased, in combination with the high velocities in the plume the convective contribution is also increased. Tilting the plasma further than 35° show only minor increase in total heat transferred to the bed for the 8MW demonstration scale kiln.

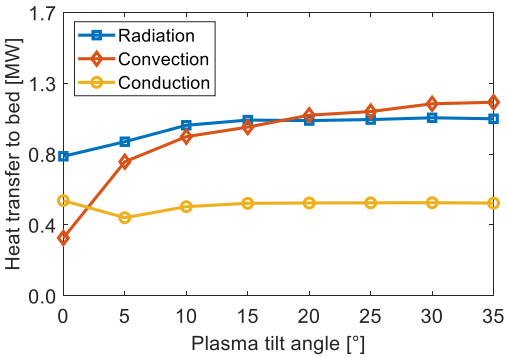

Figure 14. Heat transferred to the bed via radiation, convection, and conduction for different plasma torch tilt angles (8MW case)

Figure 15 presents the axial distribution of heat transfer to the bed, comprised of the conductive, convective, and radiative contribution, for a case with a 35° tilted and non-tilted plasma, for the $500kW_{el}$ case. Where the tilted plasma meets the bed at 2.6m from the inlet, there is a visible increase in the convective and radiative transfer, dominating the heat transfer in the hot section of the kiln. Closer to the bed inlet, conduction is the main contributor. Tilting the plasma shows a clear increase in the radiative contribution along the kiln axis, and a significant reduction in the conductive contribution close to the plasma inlet (at 2.9m from the bed inlet). Note that at 1.8m, the total net heat transfer to the bed is negative, due to the bed having a temperature

higher than that of the wall. The highest heat transfer rates are found near the bed inlet, due to the high flue gas temperatures (~1800°) interacting with the cold raw meal (~30°).

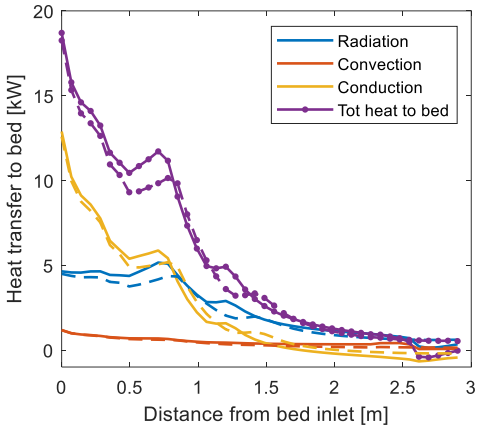

Figure 15. Heat transfer via conduction, convection, and radiation to the bed for each axial section, for a case with a 35° tilted plasma (solid lines) and a case with a non-tilted plasma (dashed lines) (500kW case)

As there is no secondary gas flow for the 500kW-case, there is no significant increase in the convective contribution, contrary to the to the 8MW-case in which there is a great improvement in the convective heat transfer due to larger gas flows.

Particles

Increasing the projected surface area of particles increases the total radiative contribution to both the bed and wall, increasing the conductive heat transfer. Figure 16 presents the radiative, convective and conductive contributions for particle addition for the $8MW_{el}$ case. The radiative contribution is increased, showing the strong impact of the increased surface area in the plasma-heated gas. Due to the higher radiative transfer, the wall temperature increases, and consequently the conductive contribution. At higher particle feeds, the convective contribution approaches negative value as temperature of the gas domain is reduced and the radiative transfer strongly dominates.

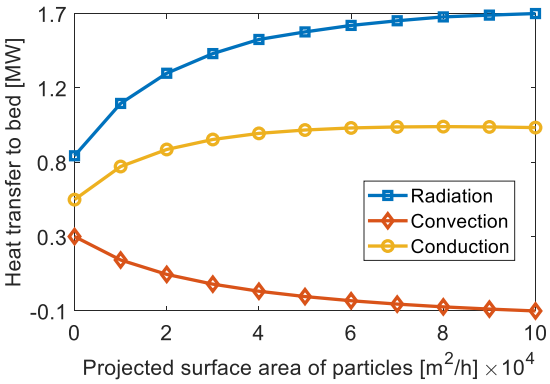

Figure 16. Heat transfer to the bed via radiation, convection, and conduction for increased particle content in the plasma gas. Note that the x-axis does not start from zero, as values become negative for high particle additions

Figure 17 presents the heat transfer contributions to the bed for the 500kW$_{el}$ case, with and without particles. A particle flow of 9500m^2/h was added, approximately corresponding to the projected surface area of a 500kW$_{th}$ coal flame. The total heat transfer to the bed, and the radiative contribution is significantly increased when particles are included. Near the bed inlet, however, the case without particles has a higher total heat transfer due to the reduced gas flue gas temperatures when introducing particles.

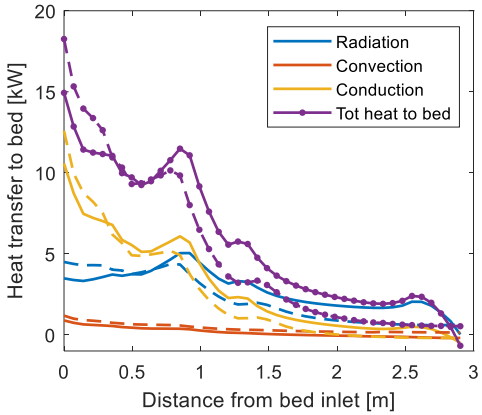

Figure 17. Heat transfer via conduction, convection, and radiation to the bed for each axial section, for a case with added particles (solid lines) and no particles (dashed lines), 500kW case.

4.1.1 Kiln heat balance

Table 2 presents the kiln heat balances for the 8MW demonstration scale kiln (with and without tilted plasma), the pilot scale kiln (500kW, with tilted plasma) and the full-scale kiln (coal). The heat balance is comprised of the total heat transfer to bed, the heat leaving the kiln with the flue gases, and shell heat losses. The heat balance for each kiln is presented as a percentage of the total heat demand in the kiln. The relative cumulative contributions of radiative, convective, and conductive heat transfer to the bed are also presented in percentage of total heat transfer to bed. For the 8MW case, tilting the plasma causes convection to become the dominating heat transfer mechanism. Nevertheless, the total radiative heat transfer to bed increases from 0.8MW to 1.06MW, but as the total heat transfer to bed is also increased the relative contribution is reduced. For the 500kW tilted plasma case, the radiative and conductive heat transfer contributions are nearly equal, showing similar proportions as the full-scale kiln. Because of the thinner wall and large surface area to volume ratio, the shell heat losses are larger for the pilot scale case than the demonstration scale and industrial kiln. Another major difference is the amount of heat leaving with the flue gases, which are larger for the plasma-heated kilns than for the coal-fired kiln.

Table 2. Heat balances of the 8MW kiln with a 0° and 35° tilted plasma, the 500kW kiln with a 35° plasma tilt, and industrial coal-fired kiln

	8MW 0° tilt	8MW 35° tilt	500kW 35° tilt	Full scale (coal) [71]
Heat transfer to bed				
Radiation:	47%	38%	46%	51%
Convection:	20%	42%	9%	5%
Conduction:	33%	20%	45%	44%
Total heat transfer to bed	22%	34%	43%	79%
Heat leaving with flue gases	77%	64%	42%	18%
Shell heat losses	2%	2%	15%	3%

Main differences between the plasma cases arise from the difference in bed material inlet temperature and the amount of secondary gas. In the pilot kiln, raw meal is fed to the kiln hence the relative heat demand of the bed material is larger as it needs to undergo calcination and clinkerisation in the kiln, compared to the 8MW case and industrial full-scale kiln where calcined meal at 900°C enters the kiln.

4.2 Wall temperature conditions

The focus of this section is to present and discuss the temperature distribution within the kiln wall and the cyclic wall temperature variation. Results are only presented for the 500kW$_{el}$ pilot scale case. The parameter study presented includes increased bed feed rate, tilted plasma, particle injection, and forced convection on the shell.

Bed feed rate

Figure 18a shows the temperature distribution in the wall for the 500kW case for two different feed rates 300kg/h (solid lines) and 350kg/h (dashed lines). The wall temperature is significantly reduced for increased feed rates, owing to the increased heat demand in the kiln. Figure 18b presents the cyclic wall temperature variation, $\Delta T_{rotation}$, for the first rotation for each axial position at the inner wall surface and at 2mm into the wall, for, 300kg/h (solid lines), and 350kg/h (dashed lines). Where calcination occurs, the temperature difference between the bed and wall is increased as there is almost no increase in the bed temperature due to the endothermic reaction absorbing all the transferred heat. The higher feed rate results in lower inner wall temperatures throughout the kiln, along with a reduced bed temperature, consequently reducing the conductive heat transfer and the cyclic temperature variation.

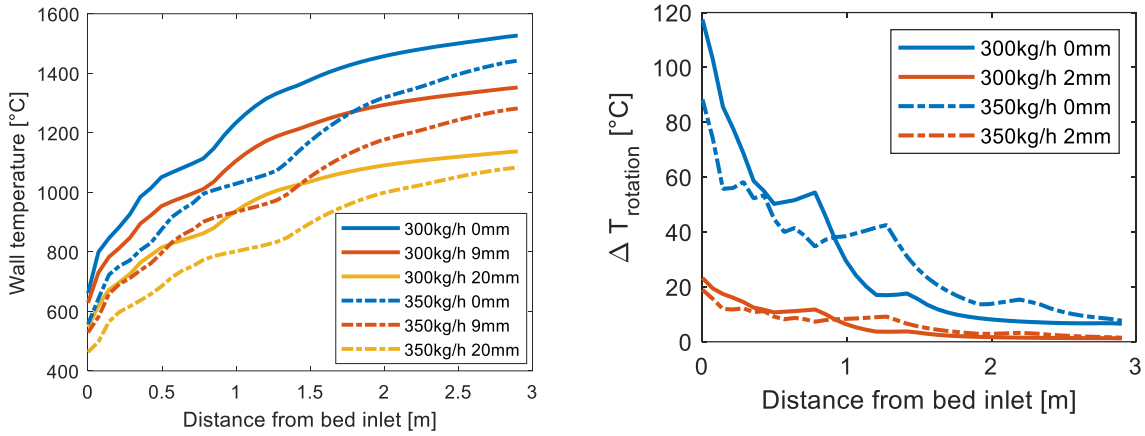

(a) (b)

Figure 18. Temperature profile of the wall and (b) cyclic variation in the wall for feed rates 300 kg/h (solid lines) and 350 kg/h (dashed lines)

Tilting

Figure 19 displays the temperature at six points inside the wall for a case with a 500kW non-tilted plasma (solid lines) and for a 35° tilted plasma (dashed lines). The inner wall surface shows a drastic temperature increase when tilting the plasma. The overall higher bed temperatures from the increased temperature causes the reduced heat transfer from the wall to the bed. Hence, the wall temperatures are higher compared to a case with a non-tilted plasma, not only at the surface but through the kiln wall.

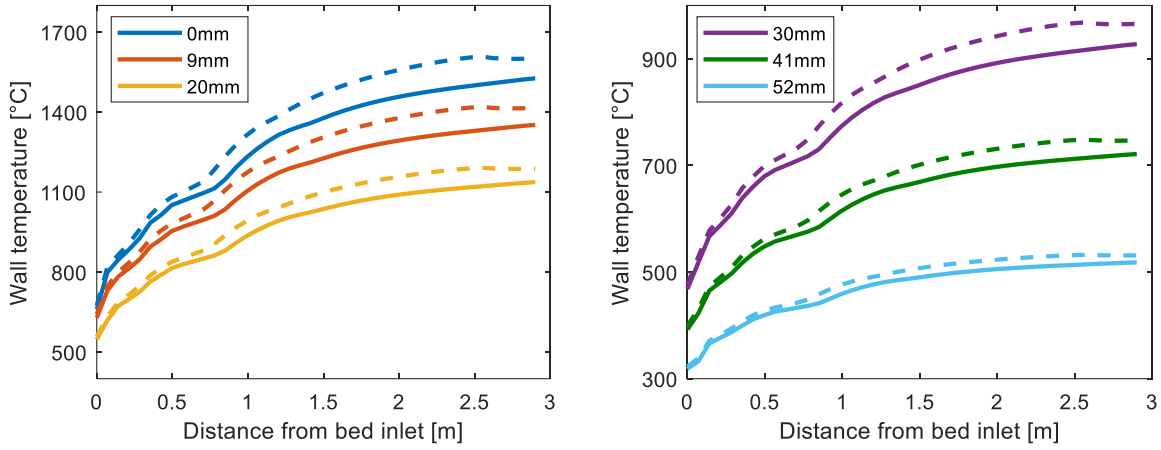

(a) (b)

Figure 19. Temperatures in the wall for the reference case (solid line) and the tilted plasma (dashed line), at positions 0-20mm (a), and 30-50mm from the inner wall surface (b).

Figure 20 presents the cyclic temperature variation for the first rotation at each axial section along the kiln axis, for a case with a tilted plasma and for a non-tilted plasma**.** Near the plasma inlet where radiation is dominating, the amplitude of the cyclic variation is reduced for the tilted plasma case compared to an axially aligned plasma. The wall temperature increases when tilting the plasma, which increases the cyclic variation near the bed inlet. However, closer to the bed outlet, the temperature difference is less, and the cyclic variation is reduced because of the decrease in the conductive contribution. Hence, the impact on the amplitude of the cyclic variation from the bed is stronger than the effect of an uneven gas temperature distribution, showing that the bed will flatten out the variation caused by the circumferentially uneven gas temperature profile.

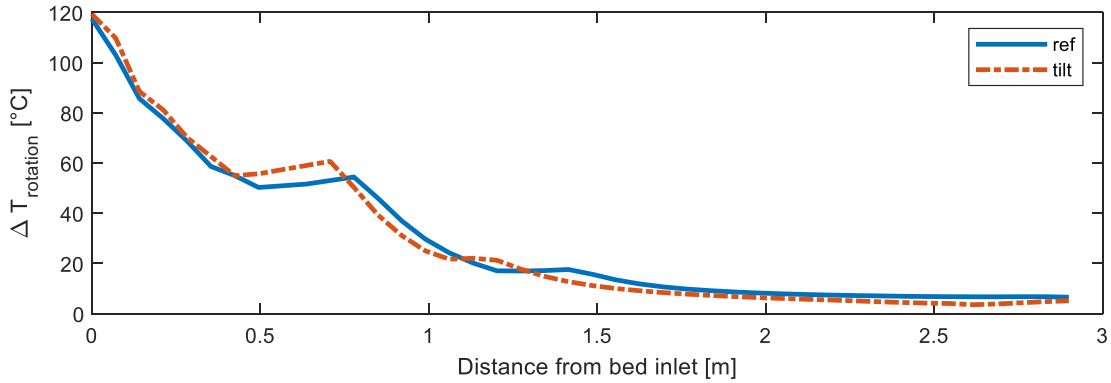

Figure 20. Wall temperature variation for each axial section in the kiln, for the reference case in solid line and the dashed line representing the tilted plasma case.

Particles

Figure 21 presents the average cyclic temperature difference for the 500kWth case with particles added to the plasma-heated gas. From the onset of calcination, there is a clear difference between the two cases, where adding particles shows an increase in the cyclic temperature variation of around 10°C. As the wall temperature reaches 1800°C near the plasma torch, there is still a conductive heat exchange between the wall and bed, causing an increased

cyclic variation compared to the case without particles, where there is no conductive heat transfer to the bed near the plasma inlet.

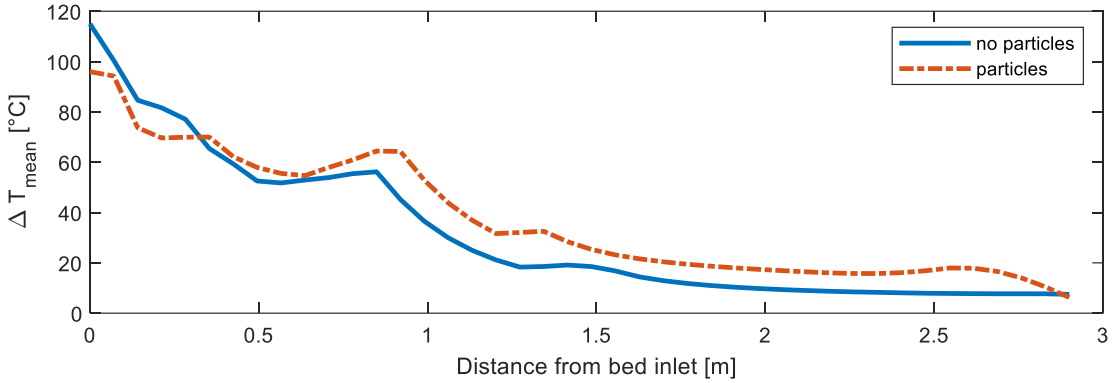

Figure 21. Average temperature difference at the inner wall surface along the kiln axis for the 500kWth case with and without particles suspended in the plasma-heated gas

Shell cooling

Figure 22 presents the average cyclic variation for the 500kWth case with and without increased shell cooling, at the inner wall surface and on the shell. The convective coefficient is increased at the angular cells before contact with the bed where the peak temperature of the inner wall appears, at all axial positions. This induces an increased cyclic variation on the shell but reduces the variation on the inner wall surface near the bed inlet. At 1m from the bed inlet, the case with increased shell cooling has a greater cyclic variation, as the bed has a smaller impact on the bed once approaching temperatures similar to the wall, the temperature cycling caused by the shell cooling has a stronger impact.

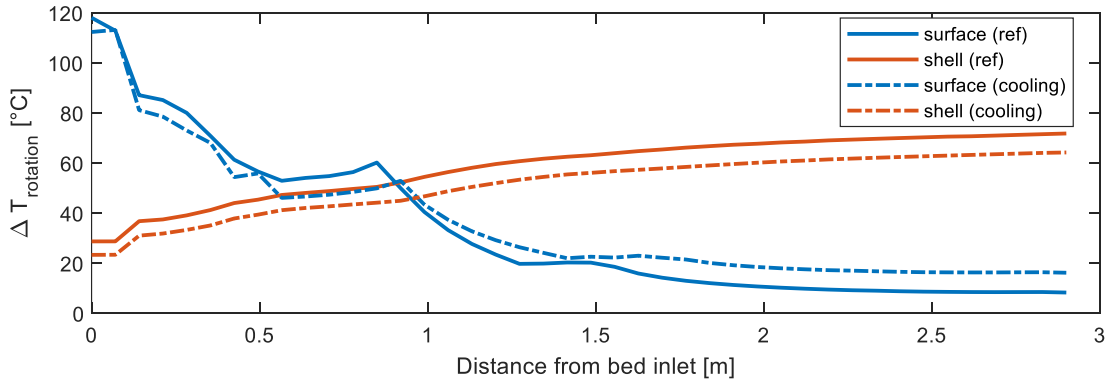

Figure 22. Average temperature difference per rotation at each axial position along the kiln length, at the inner wall surface and shell, for the reference case (solid lines) and the case with increase cooling (dashed lines).

5 Conclusions

This work has examined the heat transfer characteristics of plasma-heated rotary kilns, at both demonstration scale and pilot scale, quantifying heat transfer contributions from the gas domain and wall to the solid bed. A transient one-dimensional model has been developed to further investigate the wall temperature conditions and the interaction between the bed and rotating wall.

In **Paper I**, a plasma-heated demonstration scale kiln was studied, with down-scaled dimensions and gas flows emulating the conditions of an industrial kiln. The radiative heat transfer contribution is found to be reduced in plasma-heated systems, highlighting instead the importance of the convective contribution. The length and diameter of the kiln showed no significant improvement of the heat transfer to the bed, requiring alternative measures such as tilting the plasma torch towards the bed, or adding particles to the plasma heated gas. Due to the extreme temperatures near the plasma torch, tilting and particle addition both result in high wall temperatures, especially near the gas inlet. A lack of models describing the time dependent temperature profile in the entire kiln wall was identified and developed in **Paper II**, to allow investigation of the effect of tilting the plasma on the wall and shell temperatures. The transient 1D model enables estimations of the radial and circumferential temperature profile in the kiln wall, and how it changes with the rotation of the kiln. This thesis concludes with the following points regarding the heat transfer in plasma-heated kilns:

- Kiln dimensions play a minor role in achieving efficient heat transfer, requiring tilting the plasma towards the bed and introducing particles into the plasma heated gas to achieve favorable heat transfer conditions. Adjusting the material feed rate is important for reducing the flue gas and wall temperature, the latter especially important when the plasma is tilted to prevent over heating of the wall.
- While radiation is still the overall dominating heat transfer mechanism near the gas inlet, conduction dominates towards the bed inlet. Overall, the convective heat transfer plays an increasingly important role in plasma-heated kilns compared to coal-fired kilns. Tilting the plasma greatly increases both the convective and the radiative heat transfer, reducing the conductive contribution, while adding particles reduces the convective heat transfer, instead increasing radiation and conduction to the wall and bed.
- Tilting the plasma shows an increase in both bed and wall temperature, increasing the temperature not only at the inner wall surface but also within the kiln wall. The cyclic temperature variation in the wall near the plasma torch is reduced when the plasma torch is tilted or particles are added. Axially asymmetrical gas temperatures caused by tilting of the plasma do not significantly affect the cyclic wall temperature distribution, as the bed has a stronger influence on the amplitude of the temperature variation. Increasing the feed rate and increased shell cooling cause high cyclic wall temperature variations at the surface and in the wall, indicating that temperature cycling within the wall may not be overlooked.

Overall, this work concludes on the possibility, from a heat transfer perspective, to produce clinker in plasma-heated rotary kilns. Tilting the plasma and introducing particles improves heat transfer from the plasma-heated gas, compensating for the reduced radiative heat transfer from the gas domain when transitioning from fuel combustion to electrically heated kilns. Over-heating of the wall caused by the extreme temperatures near the plasma torch may be mitigated by carefully adjusting material feed rates and introducing shell cooling.

6 Future work

Several directions for future research are indicated by this thesis, aiming to further explore and understand heat transfer conditions in plasma-heated rotary cement kilns. The rotary kiln model and the plasma temperature profile are to be validated and compared to measurement data of the wall and/or CFD simulations. The scope should be expanded to study the impacts on process conditions, mass flows, and energy balances when transitioning from combustion to plasma heating. I have identified two main paths for continuing this research, focusing on further understanding how plasma heating (or other alternative heat sources) impacts the heat transfer interactions in the rotary kiln, and how conditions in the up- and downstream units are affected.

- Study the transient response in the rotary kiln from changing operational conditions, examining temperature distributions in the bed, wall, and gas during unstable operation or start-up/cool down of the kiln. Extending the model to include the formation and build-up of a coating layer, and its interaction with the bed motion and the onset of calcination and sintering reactions, and how new heat sources may affect the coating layer profile. The one-dimensional wall model may also be applied to other heat sources such as hydrogen. It would be interesting to study how the stability of the wall temperature variation is affected during start-up of the kiln, fluctuation in the heat release from the plasma torch, and for changes in the filling degree from a change in rotational speed and feed rate. Further comparisons with combustion-heated kilns would be valuable, and scale-up to industrial sized kilns to evaluate how the wall temperature cycling is affected in larger scale plasma-heated kilns.
- Expand the analysis to include the preheater cyclones, calciner, and clinker cooler to examine how plasma heating in the rotary kiln affects up- and downstream process units (preheater cyclones, calciner, and cooler). Specifically interesting would be to understand how reduced gas flows and high flue gas temperatures affect the mass and energy balances within the system, and to explore potential process layouts optimized for plasma heating. It would also be interesting to see how plasma-heating in the rotary kiln will impact the distribution of heat losses in the systems, and if it is possible to utilize the high flue gas temperatures in the kiln to reduce the heat input in the calciner.

References

[1] UNFCC, *Paris Agreement*, 2015.

[2] N. Darraj, and G. Bender, *Technology Brief – Carbon Neutral Energy Intensive Industries*, Switzerland, 2022.

[3] J. Moya, and A. Marmier, *Decarbonisation options for the cement industry*, Luxembourg, 2023.

[4] B. Wilhelmsson, C. Kollberg, J. Larsson, J. Eriksson, and M. Eriksson, *CemZero - A feasibility study evaluating ways to reach sustainable cement production via the use of electricity*, Sweden, 2018.

[5] F. Schorcht, I. Kourti, B. M. Scalet, S. Roudier, and L. D. Sancho, *Best Available Techniques (BAT) Reference Document for the Production of Cement, Lime and Magnesium Oxide*, Institute for Prospective Technological Studies (IPTS), Luxembourg: Publications Office of the European Union, 2013.

[6] I. Qasim, S. Mishra, A. Gunnarsson, F. Normann, and K. Andersson, "Radiative characteristics and heat transfer regime transitions in CO2-based thermal plasma jets," *Applied Thermal Engineering,* vol. 298, no. 130994, 2026.

[7] A. K. Chatterjee, *Cement Production Technology - Principles and Practice*, Florida, USA: CRC Press, Taylor and Francis Group, 2018.

[8] A. A. Boateng, *Rotary kilns: transport phenomena and transport processes*: Butterworth-Heinemann, 2015.

[9] H. G. van Oss, *Background Facts and Issues Concerning Cement and Cement Data*, U.S Geological Survey 2005.

[10] K. E. Peray, *The rotary cement kiln*, New York: Chemical Publishing Co., Inc, 1986.

[11] R. Stanev, I. Mitov, E. Specht, and F. Herz, "Geometrical characteristics of the solid bed in a rotary kiln," *Journal of Chemical Technology and Metallurgy,* vol. 49, pp. 82-89, 2014.

[12] S. H. Tscheng, and A. P. Watkinson, "Convective heat transfer in a rotary kiln," *Can. J. Chem. Eng.,* vol. 57, no. 4, pp. 433-443, 1979.

[13] X. Y. Liu, J. Zhang, E. Specht, Y. C. Shi, and F. Herz, "Analytical solution for the axial solid transport in rotary kilns," *Chemical engineering Science,* vol. 64, pp. 428-431, 2009.

[14] Y.-C. Shi, E. Specht, F. Herz, J. Knabbe, and U. Sprinz, "Experimental investigation of the axial discharging velocity of particles from rotary kilns," *Granular Matter,* vol. 13, pp. 465-473, 2011.

[15] E. Specht, Y.-C. Shi, H. Woche, J. Knabbe, and U. Sprinz, "Experimental investigation of solid bed depth at the discharge end of rotary kilns," *Powder Technology,* vol. 197, pp. 17-24, 2010.

[16] T. Haeldermans, M. A. Lataf, G. Vanroelen, P. Samyn, D. Vandamme, A. Cuypers, K. Vanreppelen, and S. Schreurs, "Numerical prediction of the mean residence time of solid materials in a pilot-scale rotary kiln," *Powder Technology,* vol. 354, pp. 392-401, 2019.

[17] X. Y. Liu, and E. Specht, "Mean residence time and hold-up of solids in rotary kilns," *Chemical Engineering Science,* vol. 61, pp. 5176-5181, 2006.

[18] S. Ngako, R. Mouangue, S. Caillat, A. Kuitche, and E. Saragba, "Numerical investigation of bed depth height, axial velocity and mean residence time of inert particles in steady state industrial cement rotary kiln: Case of Figuil Plant in Cameroon," *Powder Technology,* vol. 271, pp. 221-227, 2015.

[19] A. Chatterjee, A. V. Sathe, M. P. Srivastava, and P. K. Mukhopadhyay, “Flow of Materials in Rotary Kilns Used for Sponge Iron Manufacture: Part I. Effect of Some Operational Variables,” *METALLURGICAL TRANSACTIONS B,* vol. 14B, 1983.
[20] A. Chatterjee, A. V. Sathe, and P. K. Mukhopadhyay, “Flow of Materials in Rotary Kilns Used for Sponge Iron Manufacture: Part II. Effect of Kiln Geometry,” *Metall. Trans. B,* vol. 14, pp. 383-392, 1983.
[21] P. C. Hewlett, and M. Liska, *Lea's Chemistry of Cement and Concrete* 5th ed., Oxford, United Kingdom Butterworth-Heniemann, 2019.
[22] M. N. Pedersen, “Co-firing of Alternative Fuels in Cement Kiln Burners,” Department of Chemical and Biochemical Engineering, Technical University of Denmark, Denmark, 2018.
[23] P. Sengupta, *Refractories for the Cement Industry*, Cham, Switzerland: Springer, 2020.
[24] S. Axelsson, and K. C. Webb, *Färdplan för konkurrenskraft och nettonollutsläpp - cementbranschen*, 2023.
[25] IEA, "The challenge of reaching zero emissions in heavy industry," 2020, pp. https://www.iea.org/articles/the-challenge-of-reaching-zero-emissions-in-heavy-industry.
[26] B. Metz, O. Davidson, H. C. d. Coninck, M. Loos, and L. A. Meyer, *IPCC Special Report on Carbon Dioxide Capture and Storage*, 2025.
[27] HeidelbergMaterials. "Brevik CCS – world's first carbon-capture facility in the cement industry," https://www.brevikccs.com/en.
[28] LEILAC, *LEILAC technology - Roadmap to 2050*, 2021.
[29] E. Tsupari, K. Korpijärvi, J. Kauppinen, T. Pikkarainen, T. Leino, P. Simell, M. Lappalainen, I. Winberg, O. Katajisto, and S. Mäkikouri, *Reducing the Climate Impacts of Industry through Carbon-Neutral Energy and the Circular Economy - Decarbonate*, 2022.
[30] R. M. Jacob, and L.-A. Tokheim, “Electrified calciner concept for CO2 capture in pyro-processing of a dry process cement plant,” *Energy,* vol. 268, no. 126673, 2023.
[31] ELECTRA. "ELECTRA - the project," 05-02, 2026; https://www.electra-horizon.eu/the-project/.
[32] S. Q. Parra, and M. C. Romano, “Decarbonization of cement production by electrification,” *Journal of Cleaner Production,* vol. 425, no. 138913, 2023.
[33] M. I. Boulos, P. Fauchais, and E. Pfender, *Thermal Plasmas - Fundamentals and Applications*, New York: Plenum Press, 1994.
[34] S. Samal, “Thermal plasma technology: The prospective future in material processing,” *Journal of Cleaner Production,* vol. 142, pp. 3131-3150, 2017.
[35] E. Gomez, D. A. Rania, C. R. Cheesemanb, D. Deeganc, M. Wisec, and A. R. Boccaccinia, “Thermal plasma technology for the treatment of wastes: A critical review,” *Journal of Hazardous Materials,* vol. 161, pp. 614-626, 2009.
[36] ScanArc_plasma_technologies_AB. "Plasma systems," https://scanarc.se/products/.
[37] N. Venkatramani, “Industrial plasma torches and applications,” *Curr. Sci. ,* vol. 83, no. 3, pp. 254-262, 2002.
[38] J. Ko, T.-H. Kim, and S. Choi, “Numerical Simulation of Cement Kiln Combined with Thermal Plasma for SF6 Pyrolysis,” *Appl. Sci. Converg. Technol.,* vol. 4, pp. 93-100, 2019.
[39] I. N. Zaini, R. Svanberg, D. Sundberg, K. Bölke, J. Granqvist, C. Lille, N. Tarantino, and W. Y. a, “A pilot-scale test of plasma torch application for decarbonising the steel reheating furnaces,” *Thermal Science and Engineering Progress,* vol. 40, no. 101766, 2023.

[40] P. Amarnath, N. Nandy, B. Indumathy, and S. Yugeswaran, “Study on CO2 based thermal plasma torch and its effective utilization for material processing in atmospheric pressure,” *Journal of CO2 Utilization,* vol. 66, no. 102290, 2022.
[41] A. Gunnarsson, “Radiative Heat Transfer in Suspension-Fired Systems,” Space, Earth and Environment, Ph.D. Dissertation, Chalmers University Of Technology, Gothenburg, 2019.
[42] A. Gunnarsson, K. Andersson, B. R. Adams, and C. Fredriksson, “Full-scale 3D-modelling of the radiative heat transfer in rotary kilns with a present bed material,” *Int. J. Heat Mass Transfer,* vol. 147, 2020.
[43] J. P. Gorog, T. N. Adams, and J. K. Brimacombe, “Heat Transfer from Flames in a Rotary Kiln,” *METALLURGICAL TRANSACTIONS B,* vol. 14B, 1983.
[44] F. Herz, I. Mitov, E. Specht, and R. Stanev, “Influence of the Motion Behavior on the Contact Heat Transfer Between the Covered Wall and Solid Bed in Rotary Kilns.,” *Experimental Heat Transfer,* vol. 28, no. 2, pp. 174-188, 2014.
[45] J. P. Gorog, T. N. Adams, and J. K. Brimacombe, “Regenerative heat transfer in rotary kilns,” *Metall. Trans. B,* vol. 13, pp. 153-163, 1982.
[46] E. Ehlmé, A. Gunnarsson, K. Andersson, and F. Normann, “Heat Transfer Conditions in Hydrogen-Fired Rotary Kilns for Iron Ore Processing,” *Ind. Eng. Chem. Res.,* vol. 62, no. 37, pp. 14755-15340, 2023.
[47] E. Ehlmé, A. Gunnarsson, F. Normann, and K. Andersson, “Updated Weighted-Sum-of-Gray Gases Model Parameters for a Wide Range of Water and Carbon Dioxide Concentrations and Temperatures up to 5000 K,” *ACS Omega,* vol. 10, no. 3, pp. 2978-2985, 2025.
[48] I. Qasim, A. Gunnarsson, F. Normann, B. Wilhelmsson, A. Zether, and K. Andersson, “Heat Loss Quantification and Heat Transfer in Rotary Kilns for Calcination and Clinker Formation: From Combustion and Electrification at 150 kW to Industrial Scale,” *Ind. Eng. Chem. Res.*, 2025.
[49] S. Colin, F. Normann, C. Fredriksson, and K. Andersson, “Flame Characterization of Cofiring Gaseous and Solid Fuels in Suspensions,” *ACS Omega,* vol. 9, no. 26, pp. 28268-28282, 2024.
[50] E. Mastorakos, A. Massias, C. D. Tsakiroglou, D. A. Goussis, V.N. Burganos, and A. C. Payatakes, “CFD predictions for cement kilns including flame modelling,” *Applied Mathematical Modelling,* vol. 23, no. 1, pp. 55-76, 1998.
[51] K. S. Mujumdar, and V. V. Ranade, “CFD modeling of rotary cement kilns,” *Asia-Pacific Journal of Chemical Engineering,* vol. 3, pp. 106-118, 2008.
[52] A. Agrawal, and P. S. Ghoshdastidar, “Computer Simulation of Heat Transfer in a Rotary Lime Kiln,” *Journal of Thermal Science and Engineering Applications,* vol. 10, no. 3, 2018.
[53] A. P. Singh, and P. S. Ghoshdastidar, “Computer Simulation of Heat Transfer in Alumina and Cement Rotary Kilns,” *Journal of Thermal Science and Engineering Applications,* vol. 14, no. 3, 2022.
[54] S. Wirtz, C. Pieper, F. Buss, M. Schiemann, S. Schaefer, and V. Scherer, “Impact of coating layers in rotary cement kilns: Numerical investigation with a blocked-off region approach for radiation and momentum,” *Thermal Science and Engineering Progress,* vol. 15, 2020.
[55] C. Pieper, S. Wirtz, S. Schaefer, and V. Scherer, “Numerical investigation of the impact of coating layers on RDF combustion and clinker properties in rotary cement kilns,” *Fuel,* vol. 283, 2021.

[56] C. Pieper, B. Liedmann, S. Wirtz, V. Scherer, N. Bodendiek, and S. Schaefer, "Interaction of the combustion of refuse derived fuel with the clinker bed in rotary cement kilns: A numerical study," *Fuel,* vol. 266, no. 117048, 2020.
[57] T. Ginsberg, and M. Modigell, "Dynamic modelling of a rotary kiln for calcination of titanium dioxide white pigment," *Computers and Chemical Engineering,* vol. 35, pp. 2437-2446, 2011.
[58] H. A. Spang, "A Dynamic Model of a Cement Kiln," *Automatica,* vol. 8, pp. 309-323, 1972.
[59] J. Ryan, M. Bussmann, and N. DeMartini, "CFD Modelling of Calcination in a Rotary Lime Kiln," *Processes,* vol. 10, no. 1516, 2022.
[60] J. Ryan, "CFD Modelling of Heat Transfer and Calcination in Rotary Lime Kilns," Department of Mechanical and Industrial Engineering, University of Toronto, 2024.
[61] H. K. Versteeg, and W. Malalasekera, *An Introduction to Computational Fluid Dynamics - The Finite Volume Method*, Second ed., England: Pearson Education Limited, 2007.
[62] F. P. Incropera, D. P. Dewitt, T. L. Bergman, and A. S. Lavine, *Fundamentals of heat and mass transfer* John Wiley and Sons, 2011.
[63] P. V. Barr, J. K. Brimacombe, and A. P. Watkinson, "A heat-transfer model for the rotary kiln: Part II. Development of the Cross-Section Model," *Metall. Mater. Trans. B,* vol. 20, no. 3, pp. 403-419, 1989.
[64] G. W. J. Wes, A. A. H. Drinkenburg, and S. Stemerding, "Heat transfer in a horizontal rotary drum reactor," *Powder Technol.,* vol. 13, no. 2, pp. 185-192, 1976.
[65] E. U. Schlünder, and N. Mollekopf, "Vacuum contact drying of free flowing mechanically agitated particulate material," *Chem. Eng. Process. Process Intensif.,* vol. 18, no. 2, pp. 93-111, 1984.
[66] S. Q. Li, L. B. Ma, W. Wan, and Q. Yao, "A mathematical model of heat transfer in a rotary kiln thermo-reactor," *Chem. Eng. Process. Process Intensif.,* vol. 28, no. 12, pp. 1480-1489, 2005.
[67] F. Herz, I. Mitov, E. Specht, and R. Stanev, "Influence of operational parameters and material properties on the contact heat transfer in rotary kilns," *Int. J. Heat Mass Transfer,* vol. 55, no. 25-26, pp. 7941-7948, 2012.
[68] Y. Sonovane, and E. Specht, "Numerical analysis of the heat transfer in the wall of rotary kiln using finite element method," in Seventh International Conference on CFD in the Minerals and Process Industries, CSIRO, Melbourne, Australia, 2009.
[69] W. C. Saeman, "Passage of solids through rotary kilns: Factors affecting time of passage," *Chemical Engineering Progress,* vol. 47, pp. 508-514, 1951.
[70] A. Gunnarsson, K. Andersson, B. Wilhelmsson, A. Stjernberg, and A. Zether, "Preparational work of a small rotary kiln for cement production and plasma installation – An experimental study of the heat transfer conditions for calcination and clinkerization reactions," in Clearwater clean energy conference, Florida, 2023.
[71] A. Fakt, and M. Nilsson, "Demonstration Scale of a Rotary Kiln for Cement Production Using a Thermal Plasma: A Scaling and Heat Transfer Study," Master thesis, Department of Space, Earth, and Environment, Chalmers University of Technology, Gothenburg, Sweden, 2023.